ELEMENTA
Science of the Anthropocene

Pétron, G, et al. 2020. Investigating large methane enhancements in the U.S. San Juan Basin. *Elem Sci Anth*, 8: XX. DOI: https://doi.org/10.1525/elementa.038

RESEARCH ARTICLE

Investigating large methane enhancements in the U.S. San Juan Basin

Gabrielle Pétron[1,2], Benjamin Miller[1,2], Bruce Vaughn[3], Eryka Thorley[1,2], Jonathan Kofler[1,2], Ingrid Mielke-Maday[1,2], Owen Sherwood[3,4], Edward Dlugokencky[2], Bradley Hall[2], Stefan Schwietzke[1,2,5], Steven Conley[6], Jeff Peischl[1,2], Patricia Lang[2], Eric Moglia[1,2], Molly Crotwell[1,2], Andrew Crotwell[1,2], Colm Sweeney[2], Tim Newberger[1,2], Sonja Wolter[1,2], Duane Kitzis[1,2], Laura Bianco[1,2], Clark King[2], Timothy Coleman[1,2], Allen White[2], Michael Rhodes[1,2], Pieter Tans[2], and Russell Schnell[2]

In 2014, a satellite-based map of regional anomalies of atmospheric methane (CH_4) column retrievals singled out the fossil fuel rich San Juan Basin (SJB) as the biggest CH_4 regional anomaly ("hot spot") in the United States. Over a 3-week period in April 2015, we conducted ground and airborne atmospheric measurements to investigate daily wind regimes and CH_4 emissions in this region of SW Colorado and NW New Mexico. The SJB, similar to other topographical basins with local sources, experienced elevated surface air pollution under low wind and surface temperature inversion at night and early morning. Survey drives in the basin identified multiple CH_4 and ethane (C_2H_6) sources with distinct C_2H_6-to-CH_4 emission plume ratios for coal bed methane (CBM), natural gas, oil, and coal production operations. Air samples influenced by gas seepage from the Fruitland coal formation outcrop in La Plata County, CO, had enhanced CH_4, with no $C_{2\text{-}5}$ light alkane enhancements. In situ fast-response data from seven basin survey flights, all with westerly winds, were used to map and attribute the detected C_2H_6 and CH_4 emission plumes. C_2H_6-to-CH_4 plume enhancement correlation slopes increased from north to south, reflecting the composition of the natural gas and/or CBM extracted in different parts of the basin. Nearly 75% of the total detected CH_4 and 85% of the total detected C_2H_6 hot spot were located in New Mexico. Emissions from CBM and natural gas operations contributed 66% to 75% of the CH_4 hot spot. Emissions from oil operations in New Mexico contributed 5% to 6% of the CH_4 hot spot and 8% to 14% of the C_2H_6 hot spot. Seepage from the Fruitland coal outcrop in Colorado contributed at most 8% of the total detected CH_4, while gas venting from the San Juan underground coal mine contributed <2%.

Keywords: Emissions, Methane, Ethane, Oil and gas, Hot spot

1. Introduction

Atmospheric methane (CH_4) is a potent long-lived greenhouse gas (GHG). It is emitted by both anthropogenic and natural sources. CH_4 global sum of sources estimated using atmospheric observations as constraints was found to be 500 Tg CH_4/yr to 600 Tg CH_4/yr (Dlugokencky et al., 2009, 2011; Saunois et al., 2016; He et al., 2020).

CH_4 is the primary constituent of natural gas. It is often present in coal seams and can be coproduced with crude oil or liquid condensate. Globally, coal, oil, and natural gas extraction and the natural gas supply chain contribute about 25% of CH_4 annual total emissions, or 145 $\pm$ 23 (1σ) Tg/yr (Schwietzke et al., 2016). Anaerobic microbes decompose organic matter in landfills, wastewater, livestock manure, rice paddies, and wetlands and produce biogas, which is a mix of CH_4 and CO_2. Wetlands are the largest natural source of CH_4, contributing about one third of total CH_4 emissions globally. Enteric CH_4 is generated by methanogens in the digestive tract of ruminants. This source alone is estimated at about 100 Tg/yr

[1] Cooperative Institute for Research in Environmental Sciences, University of Colorado, Boulder, CO, USA
[2] NOAA Earth System Research Laboratory, Boulder, CO, USA
[3] Institute for Arctic and Alpine Research, University of Colorado, Boulder, CO, USA
[4] Department of Earth Sciences, Dalhousie University, Halifax, Nova Scotia, Canada
[5] Current address: Environmental Defense Fund, First Floor Bank Chambers, London, United Kingdom
[6] Scientific Aviation Inc., Boulder, CO, USA
* Corresponding author:
Email: gabrielle.petron@noaa.gov

(Gerber et al., 2013). Emissions from all microbial sources combined are estimated at 325 Tg/yr to 355 Tg/yr (Dlugokencky et al., 2011; Schwietzke et al., 2016; Tian et al., 2016). Incomplete combustion from biomass burning also results in CH_4 emissions, estimated at 43 $\pm$ 9 Tg/yr (Schwietzke et al., 2016).

The main atmospheric sink of CH_4 is oxidation by hydroxyl radicals, OH, leading to carbon dioxide, CO_2. The CH_4 global mean atmospheric lifetime is $\sim$9 years. With an atmospheric lifetime much larger than the troposphere interhemispheric $\sim$1 year mixing time, CH_4 is well mixed zonally in the background troposphere and is considered a long-lived trace gas.

Analyses of old air trapped in ice cores show that over the past 650,000 years, atmospheric CH_4 has oscillated between 350 part per billion (ppb) and 850 ppb (Etheridge et al., 2002; Loulergue et al., 2008). Due to increased emissions from agriculture and fossil fuel extraction, atmospheric CH_4 has more than doubled since preindustrial times (Etheridge et al., 2002; Loulergue et al., 2008).

The National Oceanic and Atmospheric Administration Global Greenhouse Gas Reference Network (NOAA GGGRN) has been conducting calibrated high accuracy and high precision measurements of long-lived GHG dry air mole fractions at globally distributed remote locations for over 40 years.

CH_4 measurements from air sampling at a network of locations at different latitudes in the marine boundary layer (MBL) are representative of large-scale MBL gradients. Studies of the atmospheric CH_4 budget, regionally or globally, require robust detection of small changes in CH_4 at the 1 ppb level (Dlugokencky et al., 1994).

The globally averaged marine surface air CH_4 annual mean derived from the NOAA GGGRN observations was 1,853.3 $\pm$ 0.9 ppb in 2018 (Dlugokencky et al., 2019). Since 1984, CH_4's interhemispheric difference has averaged 88 ppb, reflecting larger emissions in the Northern Hemisphere than in the Southern Hemisphere.

NOAA GGGRN measurements show that "background" CH_4 plateaued globally in the early 2000s and started rising again in 2007, reflecting an imbalance between CH_4 global sources and sinks. The year-to-year increase in global mean CH_4 has ranged between 4.6 ppb and 12.7 ppb from 2007 to 2018 (Dlugokencky, 2019). Assuming a constant lifetime, CH_4 emissions have increased stepwise since prior to 2007, reaching a $\sim$40 Tg CH_4/yr increase in 2018.

Calibrated globally distributed measurements of long-lived GHGs and stratospheric ozone depleting substances are used to track their contributions to increased radiative forcing since 1750. CH_4 is the second largest contributor to present-day total radiative forcing from long-lived GHG, after CO_2: 20% versus 66%, respectively (Butler and Montzka, 2018).

Modeling studies show that climate impacts, such as ocean warming and sea-level rise, from increased radiative forcing due to increased atmospheric burdens of long-lived GHGs will last from centuries to millennia (Zickfeld et al., 2017; Horton et al., 2018). Limiting future impacts of global climate change necessitates dramatic cuts in long-lived GHG emissions without delay (Montzka et al., 2011; IPCC, 2018; USGCRP, 2018; Nisbet et al., 2020).

Annual accounting of GHG sources and sinks by nations has long been required and encouraged by the United Nations Framework on Climate Change. This sector-based accounting often relies on bottom-up (BU) methods, or inventory calculation, which typically use reported activity counts and measured or modeled unit-level mean emission factors. Each year since the early 1990s, the U.S. Environmental Protection Agency (EPA) compiles and reports a national GHG inventory (GHGI) of annual emissions from 1990 to 2 years prior to the inventory report release year (EPA GHGI, 2018).

Atmospheric measurements of trace gases of interest can also be used in combination with measured or modeled atmospheric dispersion/transport to optimize or independently quantify emissions. These atmosphere-based quantification methods are classified as "top-down" (TD).

A few recent atmospheric composition studies have argued that the U.S. shale gas and tight oil boom may be partly responsible for increases in CH_4 observed at many sites around the globe and increases in ethane (C_2H_6) observed at several sites in the Northern Hemisphere after 2006 (Franco et al., 2016; Hausmann et al., 2016; Helmig et al., 2016; Turner et al., 2016). According to the U.S. EPA GHGI, the magnitude of O&G CH_4 emissions has not changed much over the past 10 years. Two recent analyses of NOAA GGGRN aircraft network data show a modest increase in CH_4 vertical gradient (boundary layer—free troposphere) at three sites heavily influenced by O&G operations but no detectable increase at sites in the air outflow on the U.S. East Coast (Bruhwiler et al., 2017; Lan et al., 2019).

However, over the past decade, TD studies at multiple spatial scales have found larger anthropogenic CH_4 emissions than predicted by the U.S. EPA GHGI (Miller et al., 2013; Brandt et al., 2014). Field measurement studies in U.S. O&G basins have found anomalously large emission contributions from a small fraction of facilities or unaccounted for emissions from certain operations or pieces of equipment (Allen et al., 2015a, 2015b; Lyon et al., 2015, 2016; Marchese et al., 2015; Rella et al., 2015; Subramanian et al., 2015; Brandt et al., 2016; Frankenberg et al., 2016; Bell et al., 2017).

New activity and emission data (some from studies referenced above) have led the U.S. EPA to modify the GHGI calculations for petroleum and natural gas systems CH_4 emissions since the baseline year of 1990. The 2020 GHGI recalculation for U.S. natural gas systems CH_4 emissions between 1990 and 2017, for example, resulted in an 8% decrease on average compared to the GHGI report published in 2019 and a 16% decrease for emissions in 2017 (EPA GHGI, 2020). For the year 2018, the EPA GHGI (2020) estimates of U.S. CH_4 emissions for petroleum systems and natural gas systems were 1.45 Tg/yr and 5.60 Tg/yr, respectively.

A new synthesis of O&G facility or process-level emission results, including contributions from super-emitters, derived a larger estimate for U.S. O&G CH_4 emissions of

13 ± 2 Tg CH_4/yr for 2015 (Alvarez et al., 2018). This is 60% larger than the EPA GHGI (2018) estimate. The authors also found that 85% of U.S. O&G CH_4 emissions are from production, gathering, and processing operations, which are confined in O&G producing regions (Alvarez et al., 2018).

Both BU and TD methods have inherent strengths and weaknesses. For example, super-emitter emissions are typically not considered in official BU emission inventories. Another example is that TD regional aircraft studies typically sample midday emissions. In a basin with episodic daytime emissions, it was demonstrated that aircraft-based midafternoon estimates were not representative of daily mean emissions (Schwietzke et al., 2017; Vaughn et al., 2018), but the temporal representativeness question has not been evaluated for other basins.

Another complication for TD large spatial scale CH_4 studies has to do with the quantitative attribution of estimated area emissions among various sources present in the study domain. Some regional studies have used BU estimates for non-O&G emissions (Pétron et al., 2014; Karion et al., 2013). The development of reliable measurement-based methods for the attribution of CH_4 emissions at various spatial scales is critical for the advancement of TD GHG emission budgeting and trend analysis.

$C_{2\text{-}5}$ light alkanes, also referred to as natural gas liquids, are naturally present, though in varying amounts, in thermogenic natural gas. Associated natural gas coproduced with liquid condensate and light crude oil will have higher ethane to methane (E/M) ratios than dry thermogenic gas and biogenic gas (Sherwood et al., 2013).

Several emission and air composition studies in O&G basins have shown strong correlations between methane and $C_{2\text{-}5}$ light alkanes at the surface downwind of sources or higher up in the boundary layer (Katzenstein et al., 2003; Pétron et al., 2012, 2014; Yacovitch et al., 2014; Helmig et al., 2014; Roscioli et al., 2015; Peischl et al., 2018; Kille et al., 2019; Mielke-Maday et al., 2019). Smith et al. (2016) and Mielke-Maday et al. (2019) have used enhancement ratios from survey flight in situ CH_4 and C_2H_6 measurements in the planetary boundary layer (PBL) over shale gas basins to estimate the contribution of emissions from natural gas operations to the basin total CH_4 emission estimate derived using the aircraft mass balance approach (Karion et al., 2013, 2015). This study presents a variant of the CH_4 plume attribution method based on high-frequency and high-sensitivity in situ CH_4 and C_2H_6 measurements introduced by Yacovitch et al. (2014) and Smith et al. (2015).

In 2014, a major fossil fuel producing region in the southwestern United States came into the spotlight. Kort et al. (2014) published a map of satellite-derived CH_4 column regional anomalies, which showed the U.S. "Four Corners" region (named after the intersection of four state boundaries: Utah, Colorado, New Mexico, and Arizona) was "the largest US CH_4 anomaly viewed from space."

The regional anomaly, dubbed the U.S. Four Corners CH_4 hot spot, was more specifically located over the San Juan Basin (SJB), which is home to coal, oil, natural gas, and coal bed methane (CBM) extraction. These operations are known to release CH_4, yet as mentioned earlier, U.S. O&G CH_4 emission estimates derived with different methods often disagree. Besides fossil fuel–related sources, the region is also known for CH_4 and CO_2 seepage from the Fruitland coal formation outcroppings in La Plata County in SW Colorado. The Four Corners CH_4 hot spot announcement received national news coverage, and for the local community and its leaders, it fueled an already active debate about the magnitude and impacts of local CH_4 sources.

In April 2015, several research groups funded by NOAA, NASA, and NSF deployed ground and airborne instrumentation in the SJB to further study the Four Corners CH_4 hot spot. The goals were to use coordinated in situ measurements to (1) quantify the region's total CH_4 emissions, (2) identify CH_4 sources and evaluate their contributions, and (3) document drivers of the region's CH_4 atmospheric column anomaly.

Smith et al. (2017) addressed the first goal by estimating TD total CH_4 emissions for the region using campaign data from five mass-balance flights. Their results are used in this follow-up study to address research goals 2 and 3 above. In Section 2, we give an overview of the basin topography, its CH_4 sources, and previously reported emission estimates. In Section 3, we describe the ground and airborne sampling platforms, the in situ trace gas instrumentation, and the wind profilers deployed for the campaign. Section 4 details the data analysis and main results. First, we look at boundary layer height and horizontal wind measurements and investigate the diurnal pattern in surface and boundary layer airflow at a few different locations in the mountain basin. We follow with an analysis of on-road in situ and flask air trace gas measurements, which covered major areas of the SJB and sampled CH_4 emission plumes from different sources, including various fossil fuel operations and gas seepage from the Fruitland coal outcrop in La Plata County. Sampling with an instrumented van throughout the basin at different times of the day allowed us to document the accumulation of CH_4 emissions at night in a shallow surface air layer, especially on low-wind nights in areas with nearby sources and lower elevation. In Section 4, we analyze aircraft in situ CH_4 and C_2H_6 measurements from basin survey flights. The TD attribution based on C_2H_6-to-CH_4 enhancement ratios in detected plumes provides a new breakdown of how different sources in Colorado and New Mexico contribute to the observed CH_4 and C_2H_6 hot spots. In Section 5, results are discussed in the context of existing literature. Finally, Section 6 presents the main conclusions and implications of this paper.

2. Study region and background on CH_4 hot spot

2.1. Geography

The SJB is a sedimentary basin in the Colorado Plateau in the southwestern United States (Huffman and Condon, 1993). It has many rivers and is the watershed of the upper San Juan River, which merges with the Colorado River in Utah. The region is rich in minerals and fossil

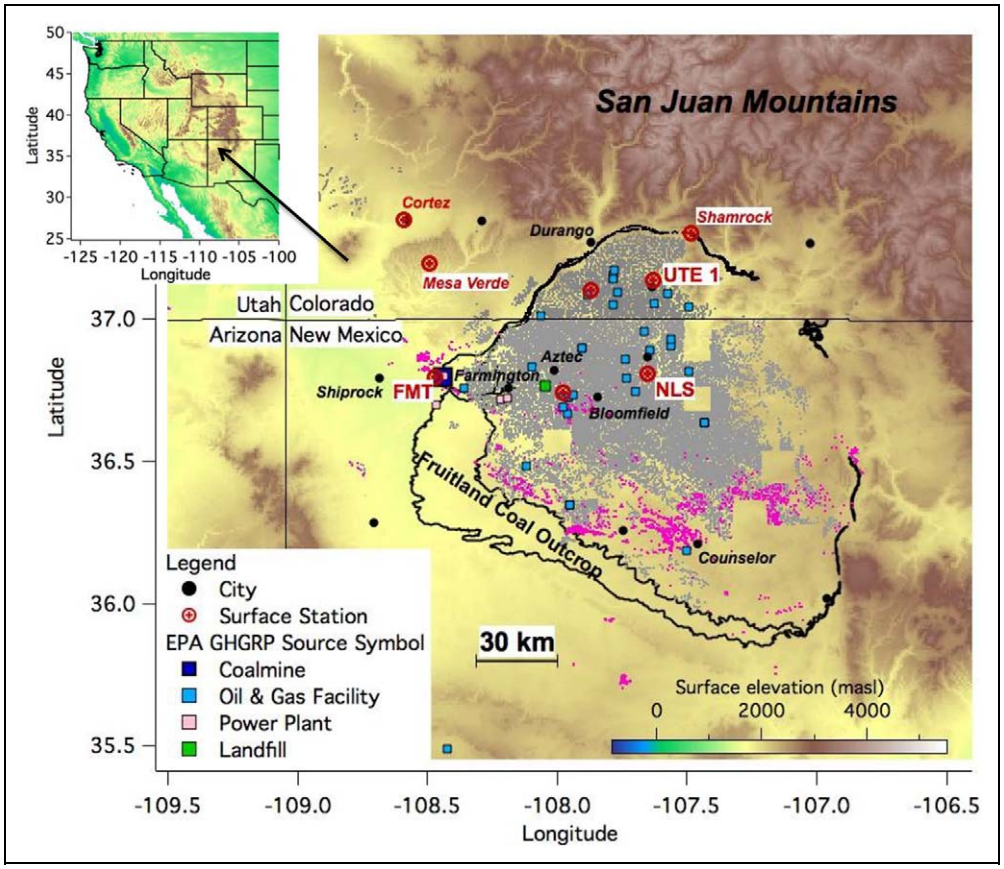

Figure 1. Topographical map of the San Juan Basin with active CBM and natural gas wells (gray dots), active oil wells (pink dots), and Fruitland coal surface outcrop (thick black line). Also shown are EPA GHGRP (2018) large point sources, long-term air monitoring sites (red circles, see **Table 2**), and locations of three wind profilers (UTE1, FMT, and NLS). The inset shows a map of the western United States colored by ground elevation, and the arrow indicates the location of the San Jan Basin. DOI: https://doi.org/10.1525/elementa.038.f1

fuels, especially coal and CBM (Fassett and Hinds, 1971; Ayers, 2003; Fassett and Boyce, 2005).

The SJB stretches over 160 km north–south and 140 km east–west. The Fruitland coal formation surface outcroppings outline most of the basin's periphery (**Figure 1**). Surface elevations range from ~1,550 meters above sea level (masl) near the Four Corners monument to almost 2,200 masl closer to the San Juan Mountain foothills. The basin is surrounded by several mountain ranges, with peaks reaching elevations above 4,000 masl to the north and over 3,000 masl to the east of the basin.

The SJB straddles the border between SW Colorado and NW New Mexico. The land and mineral rights fall under private/state, tribal, or federal ownership (Parikh et al., 2017a). According to the U.S. Census, the region's population in 2015 was close to 400,000 (Census, 2017).

2.2. San Juan Basin methane sources and hot spot

2.2.1. CH_4 sources and their emission estimates

The SJB has been a major producer of coal, CBM, conventional natural gas, and oil for decades (Figure S1, Supplementary Material Text Section 1; Barnes, 1951; Bieberman and Clarich, 1951; Murray, 1996). CBM is a type of unconventional natural gas present in an adsorbed form in underground coal deposits. CBM is typically >95% CH_4 in volume, and it is extracted using mostly vertical wells and dewatering operations (Haldar, 2018). In spring 2015, the region had two active coal mines, both tapping the Fruitland coal formation and located in San Juan County, NM. There were over 16,000 gas wells, 7,000 CBM wells, and 1,700 oil wells (Parikh et al., 2017a; Table S1) producing from a few different geological formations. The extensive gas infrastructure also includes gas pipelines and centralized gathering, processing, and compression facilities. The region has thousands of inactive or legacy wells and a large number of abandoned coal mines (Nickelson et al., 1988).

In April 2015, operations in the SJB represented 45% of U.S. CBM total production, close to 2.5% of U.S. non-CBM gas total production and only 0.25% of U.S. oil total production (Tables S1 and S2; COGCC, 2018; NM OCD Statistics, 2018; U.S. EIA, 2018a, 2018b). Close to half of the gas produced in the study area was CBM (44.3 billion cubic feet). In April 2015, there were only three active drilling rigs in the basin, all in New Mexico (Baker Hughes, 2015).

We have compiled available BU and TD estimates of CH_4 emissions of the SJB in **Table 1**. Based on data from the U.S. EPA GHGI for 2012 (Maasakkers et al., 2016), anthropogenic CH_4 emissions for the SJB add up to 0.40 Tg CH_4/yr (45.8 tonnes CH_4/h), with gas systems in New

Table 1. Summary of bottom-up (BU) and top-down (TD) CH_4 emission estimates for the San Juan Basin. DOI: https://doi.org/10.1525/elementa.038.t1

Sources	Hourly Mean Emission Estimates 10^3kg CH_4/h	Additional Information about Estimates	References
BU oil, natural gas + CBM and coal industries	43.8, 87% from NG systems and 11% from coal mining	2012 hourly mean	EPA GHGI and Maasakkers et al. (2016) (larger SJB: 36.5 to 37.5°N and 106.5 to 109°W)
BU reporting oil, natural gas, CBM companies	22.2	2015 hourly mean	EPA GHGRP, 2018
BU oil, natural gas + CBM industries	42.6 for entire basin, 43% from pneumatic devices and pumps, 34% from dehydrators, 17% from fugitive sources at well pads	2014 baseline	WESTAR/ENVIRON (Parikh et al., 2017)
BU reporting coal mining companies	3.1 to 4.9	2011 to 2016 range	EPA GHGRP (2018)
BU reporting coal power generation plants	0.28	2015	EPA GHGRP (2018)
BU reporting landfills	0.35	2015	EPA GHGRP (2018)
BU cattle—enteric fermentation and manure management	0.50	2014	USDA, 2014 and Johnson and Johnson, 1995 (SI **Table 5**),
	1.17	2012	EPA GHGI and Maasakkers et al. (2016)
BU gas seepage	14.5	2016	LTE, 2017 flux calculation based on COGCC 4 M Project flux mapping results for 2015 and 2016 in La Plata county, CO
	13.5	2015	
Total BU anthropogenic only	45.8	2012	EPA GHGI and Maasakkers et al. (2016) (no seepage)
Total BU anthropogenic + gas seepage	~60	Best available	Based on estimates above
Total TD	67.4 (50 to 77, 2σ)	2003 to 2009 mean	Kort et al. (2014)
	61.6 (39 to 85, 1σ)	April 2015	Smith et al. (2017) (5 flights)
TD for San Juan Coal mine	1.5 ± 1.5 tonnes/h	April 2015	SI Section 2.4
TD for 245 point sources	26 to 44	One week in April 2015	Frankenberg et al. (2016; five flights)

Mexico and Colorado contributing two thirds and one sixth, respectively, of this total. The WESTAR SJB inventory gives a similar estimate for O&G CH_4 emissions in 2014 (0.37 Tg CH_4/yr or 42.5 tonnes CH_4/h; **Table 1**; Parikh et al., 2017a, 2017b, see also Section 4.3.4).

Since 2007, CH_4 flux chamber measurements have been conducted in spring on a grid map over the Fruitland coal outcrop in La Plata County, CO, by consulting company LT Environmental (LTE; COGCC/LTE, 2018). The flux results show large year-to-year variability at individual measurement locations and in total detected seepage area and aggregated gas seepage magnitude.

Based on the 2016 survey total volumetric flux result (18.165 million cubic feet per day or MMcf/day) extrapolated to the entire year, LTE reports an estimated annual CH_4 emission from the outcrop in La Plata County of 125.4 Gg CH_4/yr, or 14.5 tonnes/h. Using the same derivation and LTE 2015 survey total volumetric flux result (16.903 MMcf/day), the hourly mean CH_4 source for spring 2015 is 13.5 tonnes/h (LTE, 2015, 2017). Estimates based on LTE field survey results for 2015 and 2016 are similar. However, between 2007 and 2014, LTE total volumetric flux results show large year-to-year variability with a minimum flux below 2 MMcf/day in 2010 and a maximum flux of ~11 MMcf/day in 2014 (see slide 14 in LTE, 2017). Due to the highly variable nature of gas seepage, it is expected that LTE aggregate CH_4 seepage rate is fairly uncertain.

Overall, the best available BU estimate for the SJB total CH_4 emissions around the time of the campaign is close to

60 tonnes CH_4/h (**Table 1**). The 95% confidence interval for the EPA GHGI natural gas systems CH_4 emission, the largest CH_4 source in the SJB, ranges from −19% to +30% around the inventory national estimate. At subnational scales, the emission uncertainties will be larger than for the GHGI national estimates (Maasakkers et al., 2016). A comparison of the gridded GHGI with a detailed hybrid (BU and TD) inventory for the Barnett Shale gives a relative error ranging from 30% to 50% for grid resolution going from 0.5° to 0.1° (Maasakkers et al., 2016). There is no uncertainty estimate for the Fruitland coal outcrop emission derivation from LTE.

2.2.2. Composition of emissions

Fossil fuel industry emissions in the SJB can have different chemical signatures, due to multiple formations being tapped for production (Ridgley et al., 2013), as well as varying levels of separation and processing at some facilities. Eighty-four percent of the gas produced in the northern SJB in April 2015 was CBM (Table S1), which is very dry gas with mostly CH_4, some CO_2, and no or very low nonmethane hydrocarbons (NMHC, such as C_2H_6 and C_3H_8). The southern SJB has been producing substantial volumes of both CBM and conventional natural gas and increasing, yet still modest, volumes of oil (Table S1).

CBM and conventional natural gas sample composition data for the SJB are available from the Global Inventory of Gas Geochemistry Database (Sherwood et al., 2017), which includes data from Rice (1993), the U.S. Geological Survey Geochemistry database (USGS, 2014), and the Colorado Oil and Gas Conservation Commission, among many others worldwide. C_2H_6-to-CH_4 mole-to-mole ratios (C_2/C_1) for Fruitland formation CBM samples (with reported ethane mole percent > 0.05) range between 0.05% and 12%, with a median of 0.3% in the northern SJB and a median of 3.3% in the southern SJB. For conventional gas samples, C_2/C_1 ranges between 0.05% and 18.8% for the basin, with a median of 0.4% in the northern SJB and a median of 6.6% in the southern SJB.

Accordingly, one can expect O&G emission plumes detected in the SJB to cover a large range of C_2/C_1, reflecting a complex mix of dry and wet gas operations and sources.

2.2.3. Background on Four Corners methane hot spot

Regional or local air pollution hot spots are typically caused by large localized pollution sources combined with trapping topography (basin with nearby mountain ranges) and atmospheric transport patterns, for example, recirculation from land/sea breeze, upslope/downslope winds, or surface temperature inversion at night or in winter (Baasandorj et al., 2017; Fast et al., 2007; Helmig et al., 2014; Littman et al., 1953; Oltmans et al., 2014; Reddy et al., 2016; Schnell et al., 2009; Stephens et al., 2008).

Atmospheric in situ measurements or remote sensing scans can be powerful tools to map pollution hot spots (Worden et al., 2013; Kort et al., 2014; Lawrence et al., 2015; Jacob et al., 2016) or identify and quantify larger than expected pollution sources (de Gouw et al., 2009; Frankenberg et al., 2016; Karion et al., 2013).

Kort et al.'s (2014) U.S. CH_4 anomaly map relied on retrievals of total column average CH_4 dry air mixing ratio (XCH_4, hereafter) from near infrared radiance measurements aboard the SCIAMACHY satellite (Frankenberg et al., 2006, 2011). Globally, the largest regional scale (>100 km) retrievals were observed over the tropics and in Asia and were associated with emissions from wetlands, agriculture, and coal extraction. For the western United States, Frankenberg et al. (2011) mentioned two regions with larger XCH_4 column retrievals than their immediate surroundings: the San Joaquin Valley (SJV) in California and the SJB.

High terrain regions such as the Rocky Mountains, the Himalayas, and the Andes have shorter tropospheric columns that result in smaller retrieved XCH_4 because CH_4 mixing ratios are lower in the stratosphere than in the troposphere (see figure 17 and text in Frankenberg et al., 2011). For future reference (Section 4), we also note that the SCIAMACHY/ENVISAT satellite overpass time for the SJB was midmorning, centered on 10:40 a.m. Local Standard Time (LST, or 11:40 a.m. local daylight saving time).

Kort et al.'s (2014) gridded map of regional 2009 to 2013 average CH_4 anomalies used "topography corrected" SCIAMACHY CH_4 column retrievals over the United States. Based on these maps at 1/3 degree horizontal resolution, the authors found 10 to 12 grid tiles over the SJB in Colorado and New Mexico with 25 ppb to 40 ppb enhancements over the local background XCH_4 column average. It is important to note here that the local XCH_4 background can vary by 20 ppb or more across different regions of the United States. The SJB local XCH_4 background is among the lowest in the country as the region is surrounded by mountains and less developed and industrialized areas compared to the U.S. Midwest and Eastern States.

Kort et al. (2014) concluded that the SJB was a "persistent anomalous source region," and the region became known as the "largest U.S. CH_4 anomaly viewed from space." At the very least, it might be described as "the largest local XCH_4 anomaly" derived from midmorning 2003 to 2009 SCIAMACHY retrievals. Kort et al. (2014) also estimated that the SJB emitted 0.59 $TgCH_4$/yr (0.50 to 0.67; 2σ).

In April 2015, a follow-up scientific measurement campaign took place in the U.S. Four Corners region. The main goals were to quantify and attribute CH_4 emissions using a suite of ground and airborne in situ trace gas and meteorological measurements. Smith et al. (2017) used in situ CH_4 and wind data from five flights to derive aircraft mass balance estimates of basin-wide CH_4 emissions. The annualized estimates they derived ranged from 0.31 ± 0.13 $TgCH_4$/yr to 0.84 ± 0.30 $TgCH_4$/yr. The authors averaged results from the five flights and reported an annual mean SJB TD flux of 0.54 ± 0.20 $TgCH_4$/yr. This estimate is close to Kort et al.'s (2014) mean estimate for 2003 to 2009. We note that the April 21, 2015, flight, which produced Smith et al.'s lowest mass balance CH_4 flux, only covered a portion of the SJB (see flight map in **Figure 1**; Smith et al., 2017). The low emission estimate for that flight is very likely an underestimation of the full basin emissions.

The aircraft mass balance quantification technique only provides a snapshot estimate of total midday emission for a region (Schwietzke et al., 2017). The technique does not separate and constrain contributions from individual point sources or from various source categories.

In previous O&G CH_4 TD studies, the attribution of emission estimates relied on BU/inventory information (Pétron et al., 2014; Peischl et al., 2015), on the use of additional tracers as markers for different CH_4 source categories (Smith et al., 2016; Mielke-Maday et al., 2019), or on a mix of facility-level measurements and detailed inventory activity data (Vaughn et al., 2018).

During the April 2015 campaign, some fieldwork focused on the airborne detection of individual facility CH_4 plumes with in situ measurements (coal mine and outcrop, mentioned in Smith et al., 2017) or remote sensing (Frankenberg et al., 2016; Thorpe et al, 2017). Two contracted Twin Otters equipped with NASA CH_4 partial atmospheric column remote sensing instruments AVIRIS-NG and HyTES conducted five flights over portions of the SJB. Frankenberg et al. (2016) estimated point source emissions for over 200 detected CH_4 plumes. Some of these point sources were further characterized closely in time after the detection with ground-level infrared plume imaging (Thorpe et al., 2017).

The NASA 2015 survey data set independently confirmed that there is a multitude of CH_4 emitting sources dispersed all over the SJB, including a few anomalously large sources. It also revealed that a small number of point sources contributed a large fraction of the detected CH_4 column total enhancement (Frankenberg et al., 2016).

Here, we pursue the analysis of the April 2015 ground and airborne in situ measurements to independently constrain the mix of sources and meteorological conditions contributing to the Four Corners CH_4 hot spot over the basin. In Section 3, we describe the trace gas and meteorological measurements used in the analysis.

3. Methods and data sets

3.1. Ground-based and aircraft in situ measurements

On the ground, two instrumented vehicles surveyed portions of the SJB from public access roads or with an escort on Southern Ute Indian Tribe (SUIT) and Navajo Nation roads. The NOAA Mobile Laboratory was equipped with a three species (CH_4, CO_2, H_2O) or a four species (CH_4, CO_2, CO, H_2O) cavity ring down spectrometer (CRDS, Picarro G2301 or G2401) depending on the day (due to instrumental problems) and with the NOAA Global Monitoring Laboratory (GML) programmable flask sampling apparatus (see below). The CU/INSTAAR van was equipped with a CH_4 and $\delta^{13}CH_4$ CRDS (Picarro G2132-i) and a 2D anemometer. The ground survey team members each wore a personal trace gas sensor (borrowed from the Farmington BLM office). In a few instances in the southern SJB, they did smell hydrogen sulfide (H_2S), a poisonous gas, downwind of compressor stations or well pads.

Up to five instrumented aircraft flew different patterns mostly midday (11 a.m. to 5 p.m.) and in the boundary layer over the SJB. The NOAA Twin Otter, NOAA P-3, and Scientific Aviation (SA) Mooney were each equipped with a CH_4, CO_2, H_2O CRDS (Picarro G2301), and in situ C_2H_6 spectrometer (Aerodyne; Yacovitch et al., 2014). These high-frequency, high-precision in situ C_2H_6 analyzers have been used to sample single facility or area distributed emission plumes. C_2H_6 and CH_4 plume enhancement ratios have been used to distinguish between biogenic and thermogenic sources in regions with a complex mix of CH_4 sources (Wennberg et al., 2012; Yacovitch et al., 2014, 2015; Hopkins et al., 2016; Smith et al., 2016).

The NOAA Twin Otter and Mooney also collected discrete air samples analyzed by NOAA GML. Horizontal wind speed and direction along the flight track were derived from differential GPS measurements for the Mooney (Conley et al., 2014, 2017) or derived from differential pressure measurements aboard the NOAA P-3 (Hübler et al., 1998). The CRDS analyzers in the ground vehicles and on the Mooney airplane were calibrated at the NOAA GML laboratory soon before and/or after the campaign using a suite of six gas standards spanning below and above ambient levels (1,776 ppb to 3,049 ppb for CH_4). The total uncertainty of the CRDS CH_4 measurements in the laboratory is 0.5 ppb over the calibration range.

Survey flights in a convective (well-mixed) PBL (not too deep) and under low to moderate dispersion (horizontal wind speed < 10 m/s) conditions are ideal to map and attribute emission plumes (Smith et al., 2017). Afternoon flights in the convective PBL and with steady uniform horizontal winds ($> \sim 3$ m/s) are necessary to capture horizontal gradients of CH_4 and C_2H_6 upwind and downwind of the study region for mass balance area flux calculation (Karion et al., 2013, 2015; Schwietzke et al., 2017).

The NOAA Twin Otter conducted regional mass-balance flights (Smith et al., 2017). The Mooney flew around target facilities (Frankenberg et al., 2016; Conley et al., 2017) and conducted survey flights over portions or the entirety of the SJB. The NOAA P-3 conducted two basin-wide survey flights as part of the SONGNEX aircraft campaign (Peischl et al., 2018). As mentioned earlier, two contracted Twin Otters equipped with NASA CH_4 partial atmospheric column remote sensing instruments AVIRIS-NG and HyTES conducted five flights over portions of the SJB (Frankenberg et al., 2016).

In this study, we use in situ and flask air measurements from the SA Mooney and NOAA P-3 aircraft and the two ground vehicles described above. For all platforms, scientists could visualize in situ measurements on a screen in close to real time. All sampling platforms used one or multiple GPS units to track location and time at 1 Hz. Data recorded by each instrument were merged in real time or with post-processing using the GPS location information. CH_4 in situ measurements are reported in units of dry air mole fraction, which have a total uncertainty <2 ppb at near ambient levels. All measurements are reported using the WMO X2004A CH_4 calibration scale (Dlugokencky et al., 2005; GML CH_4 Scale, 2015). Comparison plots of the in situ and flask CH_4 results for a subset of the flasks collected from the Mooney aircraft are in the supplementary material (Figure S18).

3.2. Discrete air samples

The SA Mooney aircraft and the vans were equipped with NOAA GML programmable flask packages (PFP) and programmable compressor packages. Discrete 20- to 30-s integrated air samples were collected in the PFP borosilicate flasks mostly in the boundary layer over the SJB.

More than 50 trace gases were measured in the NOAA GML laboratories and reported in units of dry air mole fraction. We use the following abbreviations: ppm = μmol mol^{-1}, ppb = nmol mol^{-1}, and ppt = pmol mol^{-1}. The NOAA GML GHG flask air analysis systems use gas-specific analyzers and custom sample inlets and data acquisition and control systems. Results are traceable to internal calibration scales derived using gravimetric methods (Hall et al., 2019). Here, we focus on the flask air analysis for CH_4 and NMHC.

Flask air CH_4 is measured using gas chromatography with flame ionization detection (Dlugokencky et al., 1994). For CH_4, each aliquot of air from a flask is bracketed by an aliquot of standard. The flask air measurement uncertainty is <2 ppb for CH_4 over the nominal standard scale range of 300 ppb to 5,000 ppb (GML CH_4 Scale, 2015). To prevent contamination of the NOAA GML analytical systems and stay within our calibration range, the NOAA van targeted air sample collection in plumes when ambient CH_4 measured with the CRDS was below 5,000 ppb. In situ CH_4 measurements above this threshold were found in plumes downwind of emitting facilities or in small valleys impacted by gas seepage from the Fruitland coal outcrop.

The NOAA GML PFP analysis includes measurements of C_2-C_6 alkanes and benzene (C_6H_6) by gas chromatography–mass spectrometry (GC-MS; system name: Perseus). These species are co-emitted by some O&G CH_4 sources. For the GC-MS, the standard protocol is to analyze air from a reference gas cylinder every five injections. For polluted samples, each flask air injection was bracketed with reference gas injections. This allowed us to closely track any changes in the instrument response when a polluted air sample was analyzed. Additionally, for flask air with CH_4 >2,200 ppb, 20% to 50% of the usual injection volume (480 mL STP) was injected to the GC-MS to reduce the impact of high mixing ratio samples on the instrument detector.

The Perseus light alkanes and benzene measurements are reported on the following calibration scales: ethane (NOAA-2015-PR1), propane (NOAA-2012-PR1), n-butane (NOAA-2012-PR1), i-butane (NOAA-2012-PR1), n-pentane (NOAA-2012-PR1), i-pentane (NOAA-2012-PR1), and benzene (NOAA-2012-PR1). Relative uncertainties associated with NMHC reported mole fractions are typically less than 5% (1 *SD*).

3.3. Horizontal wind and boundary layer height measurements

To characterize regional atmospheric transport patterns during the campaign, we deployed three wind profilers at fixed locations in the basin (**Figure 1**). Each system tracked horizontal wind speed and direction. Sunrise and sunset occurred at 6:47 a.m. and 7:41 p.m. on April 9, 2015, and 6:20 a.m. and 8:00 p.m. on April 30, 2015.

The Farmington site (FMT: 36.79N; 108.16W; 1781 masl) located on a flat portion of NW New Mexico is representative of the wind conditions on the western edge of the densely drilled south portion of the SJB. The Navajo State Park site (NLS: 36.81 N; 107.65 W; 1974 masl) is 28 miles (45.5 km) due East from FMT and in the heart of the SJB O&G operations. The southern Colorado site, near Ignacio, CO, is one of the SUIT air quality monitoring stations, UTE1 (37.14N; 107.63W; 1993 masl). It sits in the mountain foothills and is in the middle of the northern SJB natural gas and CBM operations. The San Juan Mountains peak at over 4,000 masl, ∼35 miles north of UTE1. Mountain ranges extend north to south ∼60 miles east of UTE1 and have summits above 3,500 masl.

Two NOAA 915 MHz Doppler radar wind profilers (White et al., 2015) were deployed at FMT and NLS. We use processed data from the profilers' long-range mode. The vertical resolution was 100 m, and the first reported level is at 145 m above ground level (magl). Depending on the day and time, most retrieved profiles extend to at least 2,000 magl, some reaching up to 6,000 magl. The profilers operated continuously, doing a scan for 5 min every hour, between April 8 and May 19, 2015 (no data gaps). Here, we focus on the data contemporaneous with the other measurements in April 2015.

A smaller scanning wind Doppler Lidar, WindCube 100S rented from Leosphere, was deployed at UTE1. The Lidar operated continuously from April 11 to April 30, 2015, with a profile scan every 10 min. Retrieved horizontal wind speed and direction are reported for 99 vertical levels distributed between 89 magl and 4,330 magl, but most retrieved profiles do not extend beyond 2,000 magl, and there were multiple data gaps. Vanderwende et al. (2015) describe the data processing for this type of Lidar.

4. Results

In this section, we first investigate the basin wind diurnal patterns near the surface and throughout the atmosphere's first 2 km. We then present results from the ground mobile multiple species measurements. Finally, we analyze basin survey flight in situ CH_4 and C_2H_6 measurements to attribute detected enhancements to different sources.

4.1. Horizontal wind and planetary boundary layer height (PBLH) data

Surface meteorological measurements were collected by several agencies in the SJB, and finalized data are available on the EPA AQS Data Mart web portal. Here, we analyze wind data from seven surface stations (Bloomfield, Mesa Verde, Navajo Lake, San Juan Substation, Shamrock, Ute 1, and Ute 3) and from the three profilers (UTE1, UTE3, and FMT) to investigate airflow patterns in the basin (**Figure 1** and **Table 2**).

Figure 2 shows the medians for hourly horizontal wind speed and wind direction for several altitudes up to 2,000 magl from data collected between April 9 (FMT, NLS) or April 11 (UTE1) and April 30, 2015 (all three sites). April 2015 mean wind data from colocated surface measurement systems are also shown. Note that the surface wind

Table 2. Surface air quality and meteorological variable monitoring stations in the San Juan Basin region. DOI: https://doi.org/10.1525/elementa.038.t2

Site Name	AQS Code	Site Code on Figure 1	Latitude	Longitude	Surface Elevation (masl)	Data Provider
Mesa Verde	08-083-9000	MSV	37.1984	−108.4907	2,172	National Park Service
Ute 1	08-067-7001	UTE 1	37.1368	−107.6286	1,983	SUIT Environmental Programs Division
Ute 3	08-067-7003	UTE 3	37.1026	−107.8702	1,920	
Shamrock	08-067-9000	SHM	37.3038	−107.4842	2,367	National Forest Service
San Juan substation	35-045-1005	FMT	36.7967	−108.4725	1,678	New Mexico Environment
Bloomfield	35-045-0009	BFD	36.7422	−107.9769	1,713	Department
Navajo Lake	35-045-0018	NLS	36.8097	−107.6516	1,950	

Data are available through EPA Data Mart (https://aqs.epa.gov/aqsweb/documents/data_mart_welcome.html).

diurnal patterns observed in April 2015 at the surface stations were similar for other times of the year (Figures S2 and S3).

The wind data at all monitoring sites in the area show that median horizontal winds near the surface in the SJB had a strong diurnal cycle in both direction and speed. In April 2015, surface and near surface wind speeds were minimal at night (<2 m/s to 4 m/s depending on the site) and until 11 a.m. or noon LST. At nighttime, the profiler and surface wind data had a strong vertical gradient in the wind direction from the surface to 1 km (20:00 to 9:00 LST) with NE (UTE 1) or E (FMT and NLS) surface winds sloping down from the San Juan Mountains.

Above all three sites, near surface winds switched direction between 8:00 and 11:00 LST. Profiler data for all levels below 500 magl show consistent mean winds from the W or SW for afternoon and evening hours (until 20:00 or 21:00 LST). The UTE 1 and aircraft wind data indicate some divergence in the afternoon westerly flow in the boundary layer above the SJB eastern mountain foothills (aircraft wind data are not shown here but are included in data files).

Above 500 magl, the wind profiler data show uniform winds throughout the day and night, from the SSW (200 to 210°) above UTE 1 or from the SW to W above FMT and NLS (**Figure 2**). The horizontal wind speed between 500 magl and 2 km agl has a smaller diurnal cycle, with a minimum between 3 m/s and 4 m/s midmorning, when the daytime boundary layer is developing. On most clear-sky days, by 12:00 to 14:00 LST, the boundary layer is convective and well developed, and the horizontal wind speeds throughout the PBL are homogenous. In the afternoon, the typical mean horizontal wind speed in the PBL is 5 to 6 m/s above FMT and NLS and 3 to 4 m/s above UTE 1.

The daytime convective PBLH was estimated above FMT and NLS from the analysis of the structure of the NOAA Doppler radar-derived vertical wind velocity and atmosphere refractive index, as described in Bianco et al. (2008). Between April 9 and May 1, 2015, the convective PBLH was successfully retrieved over FMT and NLS typically between 9 a.m. and 5 p.m. LST.

The profiler retrievals show that the PBL growth pattern and peak height varied greatly between days at FMT and NLS (Figure S4). The earliest valid PBLH retrievals at 8:00 LST for the FMT profiler have readings below 450 magl. At 11 a.m. LST, the mean PBLH was 490 $\pm$ 250 magl at FMT (22 estimates between April 9 and May 1, 2015) and 470 $\pm$ 225 magl at NLS (16 estimates). The PBLH daily maximum ranged between 1,000 and 4,000 magl above both locations. PBLH could not be estimated during very cloudy conditions or when turbulent mixing was not strong enough, which explains the shorter PBLH time series on several days.

For the 6 days with PBLH profiler data extending in the evening at NLS and/or FMT, we see that the boundary layer started collapsing between 5 p.m. and 6 p.m. LST. In the late afternoon, rapidly declining sun radiation leads to the sudden halt of convective atmospheric mixing above the Earth's surface and the resulting collapse of the atmosphere daytime mixed PBL. At night, the atmosphere surface layer depth is a couple hundred meters deep at most. Vertical mixing in this nocturnal surface layer (typically induced by horizontal wind friction) is very limited in the SJB due to very low surface wind speeds (**Figure 2** and Figure S2), and therefore at night, surface CH_4 emission plumes are "trapped" and can lead to large surface enhancements near sources, as shown in the next section.

4.2. Ground in-situ and discrete sample measurements

We conducted ground mobile measurement on 14 different days between April 11 and April 29, 2015, mostly from public roads. Prior consent was obtained to conduct air measurements from roads on Native American land. Several drives or portions of drives were also conducted with an official escort on Navajo Nation land and SUIT land.

The van's fast response CO_2, CH_4, and CO CRDS measurements were used to map CH_4 levels at the surface in different parts of the basin and to locate and identify CH_4 point sources and direct discrete air sample collection in emission plumes for additional chemical composition data.

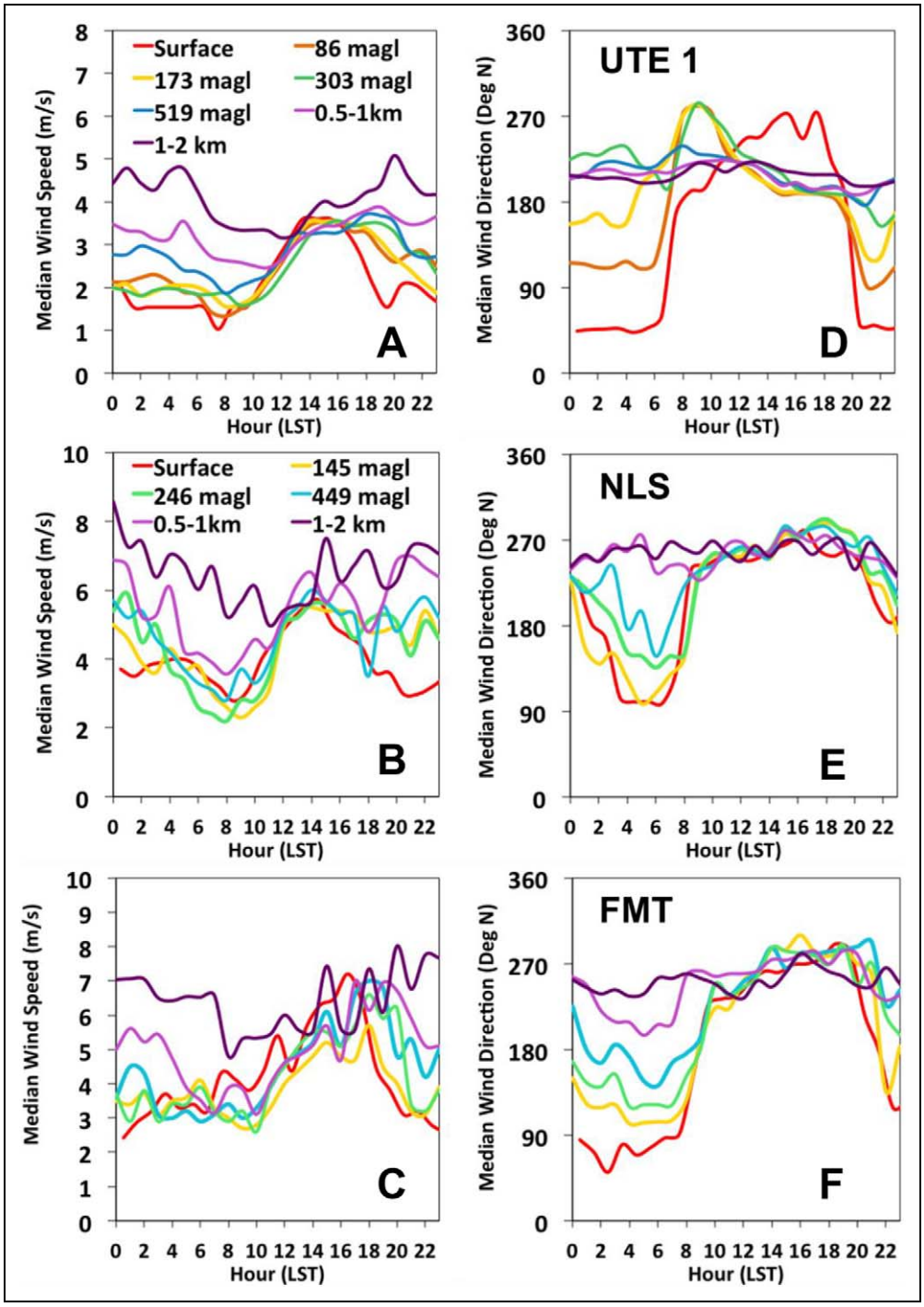

Figure 2. Diurnal cycle of median horizontal wind speed (Plots A to C) and median horizontal wind direction (Plots D to F) based on data from the wind profilers at the UTE1, NLS, and FMT locations. Surface station data are shown in red, and wind profiler data for various retrieval levels are shown in other colors (same heights for FMT and NLS). Times shown are Local Standard Time (LST = Local Time-1). DOI: https://doi.org/10.1525/elementa.038.f2

Speciated trace gas emission inventories rely on industry or EPA data to derive a mean emission composition signature for different sources in a sector or basin. As we were planning the fieldwork, we did not have access to recent spatially relevant emission composition data. Therefore, we decided to collect air samples in CH_4 emission plumes intercepted with the van for a subset of sources.

Below, we describe examples of surface hydrocarbon enhancements observed along those drives. Later, the surface air sample results support the interpretation of the aircraft in situ and discrete air measurements, which typically reflect emissions from a mix of point and area sources in a larger spatial footprint than the van's samples.

4.2.1 Methane sources and their emission chemical signatures

Significant enhancements of surface CH_4 detected by the NOAA van instrument downwind of a facility are

interpreted as emission plumes from the upwind facility. Typically, the emission plumes had peak CH_4 enhancements hundreds to thousands of ppb above the local background (1.8 ppm to 2.0 ppm CH_4). To get an emission source chemical signature, three or more flask samples were collected with the van in local background air and downwind in the facility emission plume(s) to capture different enhancement levels in a 15-min to several-hour-long sampling time window. A constant local background and emission composition is assumed for an entire sampling window downwind of a particular facility. The NOAA van collected air in flasks while stationary with the engine turned off and away or upwind from local road traffic.

Table 3 lists the location, date, and time, as well as the C_2H_6 to CH_4 and C_3H_8 to C_2H_6 mixing ratio correlation results for sampled plumes at 20 locations in the SJB and for background samples in the nearby Paradox oil producing basin in SE Utah.

Gas seepage plumes were sampled at five locations along the Fruitland coal outcrop in La Plata County where CH_4 emissions have been observed and reported (LTE, 2015). In remote outcrop sampling locations (April 12 and 14 outcrop locations #4 and 5 in **Table 3**), C_2H_6 in samples with elevated CH_4 (2.5 ppm to 5.2 ppm) was less than 1 ppb above the local background and was uncorrelated with CH_4 or other light alkanes (Figures S5 to S8). As a result and for the rest of this paper, we assume that SJB outcrop gas seepage has no C_2H_6.

Other sampling locations were either downwind of known facilities and potentially large point sources of CH_4 (San Juan coal mine air shaft, compressor stations, and processing plants) or happened in emission plumes encountered during a survey drive (e.g., downwind of active well pads).

On eight drives in April 2015, we collected three to seven discrete air samples in CH_4 plumes downwind of eight active well pads, three compressor stations, and two processing plants. These O&G facility plumes have highly correlated C_2H_6 and CH_4 with slopes spanning a wide range from very dry gas <1% in CBM producing areas to wet gas ($\sim$17%) in the oil producing region near Counselor (**Table 3**).

Air samples were collected in Durango and its vicinity in La Plata County in areas with known outcrop gas seepage on April 11 to 14, 2015 (Figures S5 to S7). The sample analysis results show no clear correlation between CH_4 and C_2H_6 (40 samples, Figure S8A). These samples, however, show strong correlations between the $C_{2\text{-}5}$ alkane levels with similar slopes as the chemical signatures for air samples collected near O&G operations in the SJB: C_3H_8-to-C_2H_6 slope of 0.38% (Figure S8B) and iC_5H_{12}-to-nC_5H_{12} slope of 1.1 ppb/ppb. This suggests that the background air in Durango and the nearby surroundings is likely impacted by hydrocarbon emissions from O&G operations in the SJB.

On April 19, 2015, the NOAA van CRDS detected up to 16 ppm CH_4, $\sim$¾ mile east and downwind of the San Juan coal mine air shaft. C_2H_6 and CH_4 were strongly correlated in seven discrete air samples with a slope of 0.9% (R^2 of 0.98, **Table 3**; Figures S9 and S10). On April 21, 2015, the NOAA van sampled surface air from dirt roads near the Navajo surface coalmine operations, including Indian Service Road 5082 (Figures S11 and S12). In situ CH_4 measurements were close to background levels (1,880 ppb to 1,910 ppb) the entire time. Four flasks collected during that time had CH_4 and C_2H_6 ranging between 1,880 ppb to 1,906 ppb and 1.7 ppb to 2.7 ppb, respectively, which are very close to background levels. These findings are supported by data from targeted aircraft flights over both active coalmines.

The WESTAR O&G emission inventory project gathered operational data from O&G companies active in the basin. Based on the SJB survey data for 2014, 94% of active CBM and gas wells in the basin had a wellhead gas compressor engine (90% rich burn/10% lean burn) with some form of emission controls, and 99% of oil wells had a gas-fueled rich burn artificial lift engine (Parikh et al., 2017a, 2017b). In the SJB, natural gas engines are the largest O&G source of NOx (Parikh et al., 2017a, 2017b).

On a few road surveys in April 2015, the NOAA van was close enough downwind of an O&G facility to isolate CH_4 emission plumes with elevated combustion markers CO_2 and CO. These plumes may have been the result of a mix of on-site gas venting, leaks, and incomplete combustion emissions from an on-site natural gas-fired engine. Using 10-s moving averages of the CRDS 0.5 Hz CH_4, CO_2, and CO measurements, we report facility plume emission ratios for five centralized compressor stations, one gas plant complex, and 11 well pads (**Figure 3**, Table S6). CH_4-to-CO_2 (CO-to-CO_2) correlation slopes for intercepted plumes with $R^2 > 0.5$ ranged from 0.09 ppm to 2.4 ppm CH_4/ppm CO_2 (2.3 to 93 ppb CO/ppm CO_2) for emission plumes from large NG facilities and from 0.023 ppm to 11.6 ppm CH_4/ppm CO_2 (non-detectable to 1,467 ppb CO/ppm CO_2) for emission plumes from well pads. Some of these intercepted plumes were clearly attributable to compressor engine emissions (CS#1–5 in Table S6) or to natural gas-driven compressor or pumpjack on a well pad (WP#1,2,4,7,9 in Table S6), given the facility equipment layout and the predominant winds at the time of the sampling.

The NOAA Mobile Laboratory brief fenceline sampling of emission plumes from sites with natural gas combustion engine covered a small fraction of the SJB O&G engine population and emissions. At each site, the sampling occurred for short periods as back then O&G engine emissions had not been identified as a study target. Also, the mobile surface air sampling, despite being random in term of roads traveled, more easily picked up anomalously large enhancements such as the ones reported here.

Despite these limitations, we compare our observed emission plume ratios with the WESTAR inventory emission factors. **Figure 3** shows that, especially for CH_4/CO_2, the observed ratios are several orders of magnitudes above the WESTAR inventory emission factors for point/large engines (2.10^{-4} ppm CH_4/ppm CO_2 and 2 ppb CO/ppm CO_2) and nonpoint/small engines at well pads (5.10^{-5} ppm CH_4/ppm CO_2 and 27 ppb CO/ppm CO_2).

Table 3. Results from facility emission plume sampling with National Oceanic and Atmospheric Administration GML flasks. DOI: https://doi.org/10.1525/elementa.038.t3

Samples Date	Time Window UTC	Source Type or Name	Latitude	Longitude	Number of Flasks	C_2H_6-to-CH_4		C_3H_8-to-C_2H_6		Min and Max CH_4 (ppb)	Min and Max C_2H_6 (ppb)
						Slope	R^2	Slope	R^2		
April 11, 2015	21:34 to 2:44	Fruitland outcrop #1	37.291	−107.798	3	None	—	0.33	0.97	1,947 to 2,397	3.8 to 4.0
April 11, 2015	21:50 to 22:06	Fruitland outcrop #2	37.290	−107.797	4	None	—			2,017 to 3,797	5.3 to 5.7
April 11, 2015	22:26 to 22:40	Fruitland outcrop #3	37.236	−108.867	4	None	—			1,944 to 2,990	4.5 to 4.6
April 12, 2015	14:35 to 15:56	Fruitland outcrop #4	37.316	−107.668	8	0.03%	0.74	None	—	2,051 to 5,213	1.6 to 2.7
April 14, 2015	15:49 to 16:03	Fruitland outcrop #5	37.105	−108.070	4	None	—	None	—	2,652 to 3,452	4.2 to 4.9
April 13, 2015	19:55 to 20:10	Gas well	36.992	−107.514	3	0.34%	—	0.22	—	2,055 to 3,220	6.5 to 10.5
April 14, 2015	23:37 to 0:26 (next day)	San Juan Gas Plant	36.764	−108.361	7	2.20%	1	0.21	0.92	2,063 to 4,749	5.7 to 65
April 16, 2015	20:39 to 21;25	Well pad B	36.874	107.990	3	2.20%	—	0.16	—	1,916 to 3,125	2.8 to 30
April 16, 2015	21:47 to 22:05	Well pad C	36.870	−107.985	3	8.10%	—	0.29	—	2,240 to 3,123	27.4 to 100
April 16, 2015	23:01 to 23:21	Well pad E	36.882	−108.042	3	10%	—	0.32	—	2,053 to 5,839	10.5 to 390
April 16, 2015	23:38 to 23:53	Well pad F	36.909	−108.085	3	2.40%	—	0.34	—	2,132 to 2,309	8.0 to 12.2
April 17, 2015	22:00 to 22:40	Well pad	36.651	−107.940	6	2.65%	1	0.20	1	1,937 to 2,985	2.9 to 30
April 17, 2015	1:34 to 1:56 on 4/18	Well pads near counselor	36.217	−107.512	5	16.8%	0.94	0.51	0.67	2,094 to 6,848	42.6 to 870
April 19, 2015	18:56 to 20:10	Underground San Juan coal mine	36.796	−108.375	7	0.90%	0.98	0.10	0.76	2,005 to 2,801	3.8 to 10.9
April 21, 2015	16:17 to 16:32	Williams Plant	37.144	−107.787	4	12.40%	1	0.54	0.98	1,979 to 2,844	2.0 to 110
April 21, 2015	19:26 to 21:07	Navajo surface coal mine	36.527	−108.483	4	—	—	—	—	1,880 to 1,905	1.7 to 2.7
April 21, 2015	22:45 to 1:18	Compressor GCP1-3026	36.724	−107.850	7	9.20%	0.99	0.34	0.99	1,900 to 3,317	3.1 to 136
April 23, 2015	19:42 to 19:54	Turley compressor	36.769	−107.791	5	8.10%	0.99	0.33	—	1,926 to 4,748	6.2 to 233
April 28, 2015	17:01 to 19:18	Utah Paradox Basin, background in area			6	6.10%	0.96	0.47	0.83	1,904 to 1,965	2.6 to 6.1
April 29, 2015	20:35 to 20:57	Gas well pad	37.013	−107.628	4	1.75%	0.95	0.08	1	1,993 to 2,479	5.3 to 13.7
April 29, 2015	21:47 to 22:07	Compressor	36.815	−107.619	3	1.61%	—	0.162	—	2,457 to 5,586	14.2 to 65

R^2 is only reported for sites with four or more discrete samples. Slope unit is ppb/ppb.

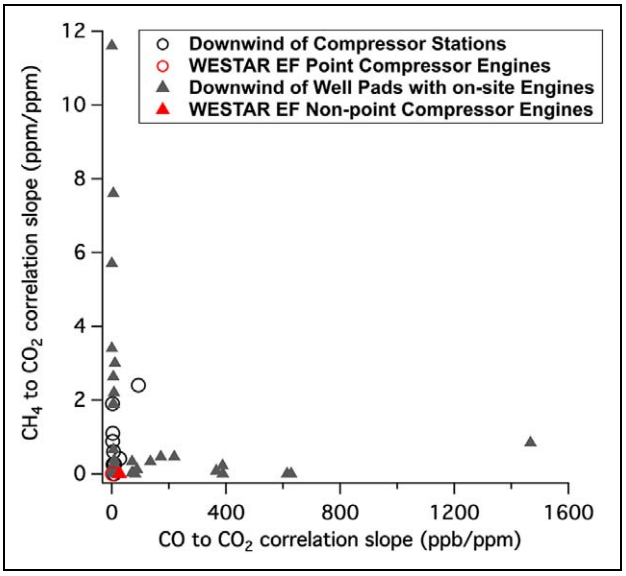

Figure 3. Combustion efficiency results based on downwind plume measurements by CRDS in the SJB in April 2015 (black symbols). WESTAR inventory emission factors are shown in red. DOI: https://doi.org/10.1525/elementa.038.f3

Our results suggest that upstream and midstream facilities with natural gas burning engines may have temporally varying combustion efficiencies and that some could have significant leaks. More coordinated and representative research for a representative subset of sites would be necessary to better characterize and mitigate emissions and fat tail drivers for CH_4, VOCs, CO, and other air pollutants from enhanced recovery operations with natural gas engines and from centralized gathering and processing stations.

4.2.2. Durango to Farmington transects and nighttime CH_4 accumulation at the surface in the SJB

The North–South road between Durango, CO, and Aztec (or Farmington), NM, was driven multiple times during the campaign. **Figure 4** shows the change in surface CH_4 levels for morning, afternoon, and evening drives, respectively. Small-scale CH_4 spikes of several hundred ppb to several ppm above baseline levels attributable to nearby point source emissions were recorded along all drives.

Three drives completed before 10 a.m. LT (April 17, 20, and 29, 2015) show higher overall CH_4 levels for both the baseline and local (100 m to a few kilometers long) enhancements compared to later in the day drives. On these drives, CH_4 baseline levels are at background levels at 1.9 ppm to 2 ppm in Durango (37.27N) and then start increasing slowly south of 37.2N to reach 2.3 ppm to 2.8 ppm depending on the day. Baseline CH_4 levels increase more sharply around 37.1N to reach over 4 ppm where the Animas and Florida rivers meet near 37.06N (near Hwy 550 and county roads 213 and 110). On the New Mexico side, the two drives with measurements obtained before 8 a.m. LT have baseline CH_4 levels ranging between 2.9 ppm and over 10 ppm (detected near Aztec, NM).

Afternoon and evening measurements also show spatial and day-to-day variability in baseline CH_4 levels but of much smaller magnitude. Measured baseline CH_4 levels along the transect were contained between 1,880 ppb and 2,000 ppb between noon and 5 p.m. and between 1,888 ppb and 2,100 ppb between 6 p.m. and 10 p.m. (all LSTs).

To further look into the accumulation of CH_4 at the surface in the SJB at nighttime, the CU/INSTAAR van conducted six back and forth transects between Durango and Aztec, starting at 10 p.m., 2 a.m., and 6:48 a.m. on April 19 to 20, 2015. The mean surface winds between 10 p.m. and 8 a.m. that night at the five monitoring stations ranged from 0.7 m/s at Shamrock to 2.5 m/s at the San Juan Substation. In situ CH_4 from the different drives is described in SM Section 2.4 and shown in Figure S13. The later transects between 2:00 a.m. and 7:25 a.m. show increased CH_4 south of 37.2N compared to the back and forth transect between 10 p.m. and 11 p.m. The CU/INSTAAR van took different roads for the northern portion of transects going southward and northward. County Road 213 was taken for the northbound transects. It follows the Animas River and is at a lower elevation compared to Highway 550. Surface CH_4 levels were significantly higher along CR213.

On April 20, 2015, the NOAA van also took advantage of the low surface winds to map CH_4 and NMHC accumulation along a loop between Durango-Farmington-Navajo Lake-Durango (4 a.m. to 8:30 a.m. LST) on major roads and close to major riverbeds. The NOAA van in situ CH_4 measurements and analysis results for 17 flasks collected along the drive are shown in Figures S14 and S15. Surface CH_4 was elevated for most of the drive, and CH_4 and NMHC mixing ratio enhancements in flasks collected in New Mexico are strongly correlated. The van measurements illustrate the increased impact of local CH_4 sources on surface air composition at night and early morning when limited air circulation leads to the pooling of emissions near sources, especially in low elevation portions of the basin.

4.2.3. Ground flask results summary

To further investigate the air composition in the basin, discrete air samples were collected in NOAA flasks on the ground (212 samples) and by aircraft (101 samples; **Figure 5**). Unfortunately, the NOAA van did not sample surface air in the SJB uniformly. The lack of paved access roads and limited sampling time did not give us the opportunity to explore with the van a large area south of Bloomfield and north of Counselor. Boundary layer air over this area was sampled, however, by aircraft (Section 4.3). In this section, we will focus on summarizing the main findings for the multi species analysis of surface air samples.

Figure 6 (Panels A to D) shows correlation plots for CH_4 and several NMHC analyzed by NOAA GML in the surface flasks. The flask data show a large spread in C_2H_6-to-CH_4 correlation slopes with lower slopes (<5%) for samples collected in the northern SJB, where CBM and dry natural gas are produced and where there is degassing of CH_4 from the Fruitland coal outcrop. Three samples

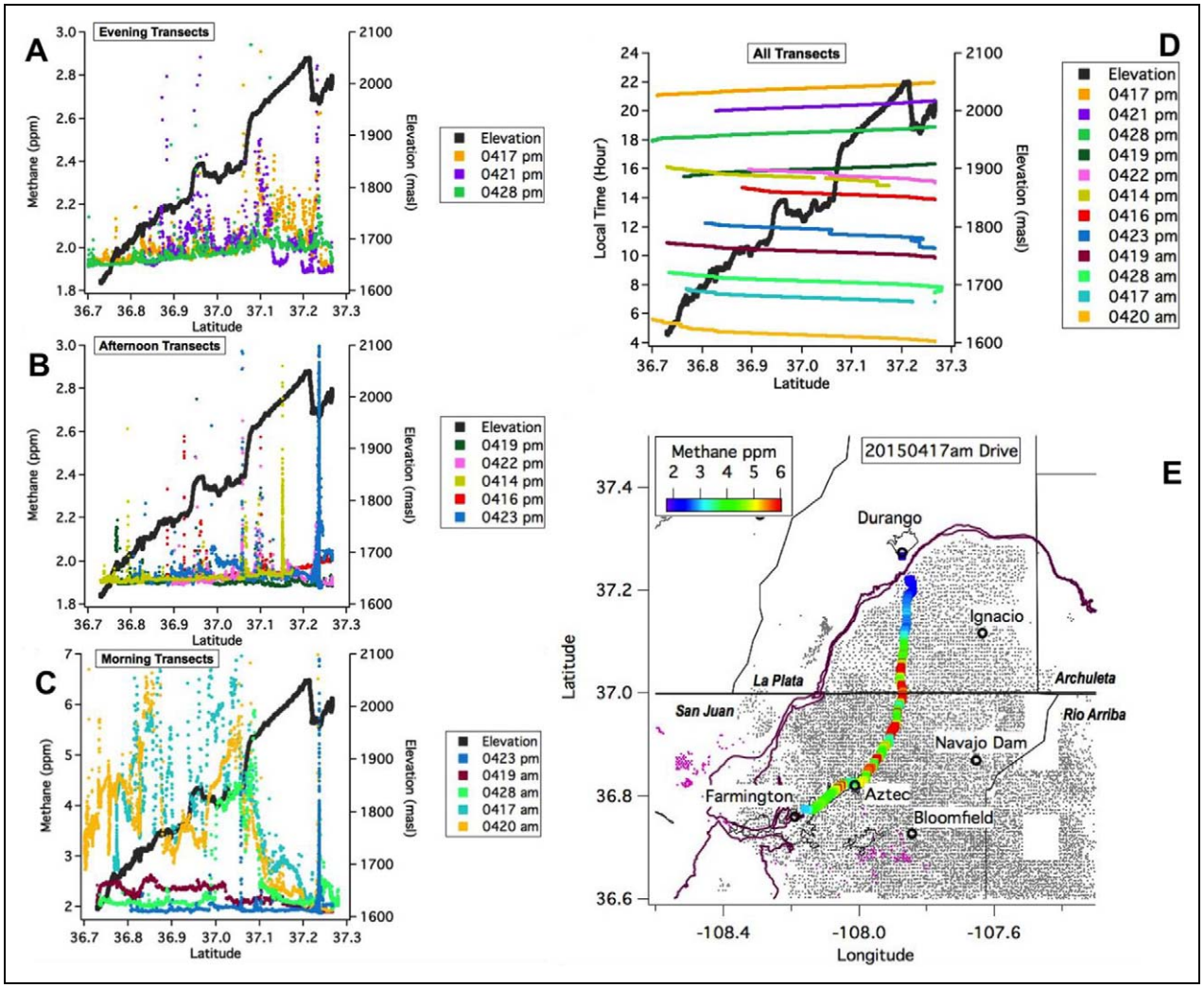

Figure 4. Surface CH_4 along a Durango to Aztec or Durango to Farmington transect on different days and at different times of the day: A/morning, B/afternoon, and C/evening. Note different *y*-axis range for A to C. For each transect, the local drive time (LT = LST + 1) as a function of latitude is shown in Plot D. The transect route, color-coded by the measured CH_4 from an early drive on April 17, 2015, is shown in Plot E. On this map, active gas wells appear as gray dots and active oil wells as pink dots. The CH_4 *y*-axis range for Plot C is truncated at 7 ppm (highest levels reach over 30 ppm) such that one can better see the CH_4 levels for the midmorning and midday transects. The midday transect (04:23 p.m.) is shown in both B and C. Two transects (April 28 and April 19) are closest to the SCIAMACHY overpass time, shown in C and D. DOI: https://doi.org/10.1525/elementa.038.f4

collected downwind of the Williams natural gas processing plant near Ignacio, CO, have a C_2H_6-to-CH_4 correlation slope of 12.4% (**Table 3**). The facility treats raw natural gas from Colorado and New Mexico and is likely a complex mix of sources with different emission signatures. Air samples collected in New Mexico had a much wider range of C_2H_6-to-CH_4 correlation slopes from 0% to >15%. In the next section, this observation is confirmed by the more spatially extensive aircraft in situ CH_4 and C_2H_6 measurements over the SJB.

4.3. Aircraft in situ and discrete sample measurements

Two aircrafts equipped with fast-response highly sensitive CH_4 and C_2H_6 measurements mapped levels in the PBL throughout the SJB. They mostly sampled the convective boundary layer air between 11 a.m. and 5 p.m. LT on clear-sky days.

On steady wind days, mass balance downwind transects were conducted later in the afternoon to capture the outflow from "fresh" (as opposed to "accumulated") emissions. CH_4 enhancements measured in the PBL downwind on the north or eastern edge of the SJB during mass-balance flights reached 30 to 90 ppb (**Figure 1** in Smith et al., 2017). These downwind levels are a direct function of upwind cumulative CH_4 emissions, how fast the airmass traveled over the source region, and the depth of the PBL (see details on aircraft mass balance method and implementation in Karion et al., 2013).

Here, we analyze PBL (<3,000 masl) CH_4 and C_2H_6 enhancements for five SA Mooney and two NOAA P-3 survey flights during midday and afternoon hours and for

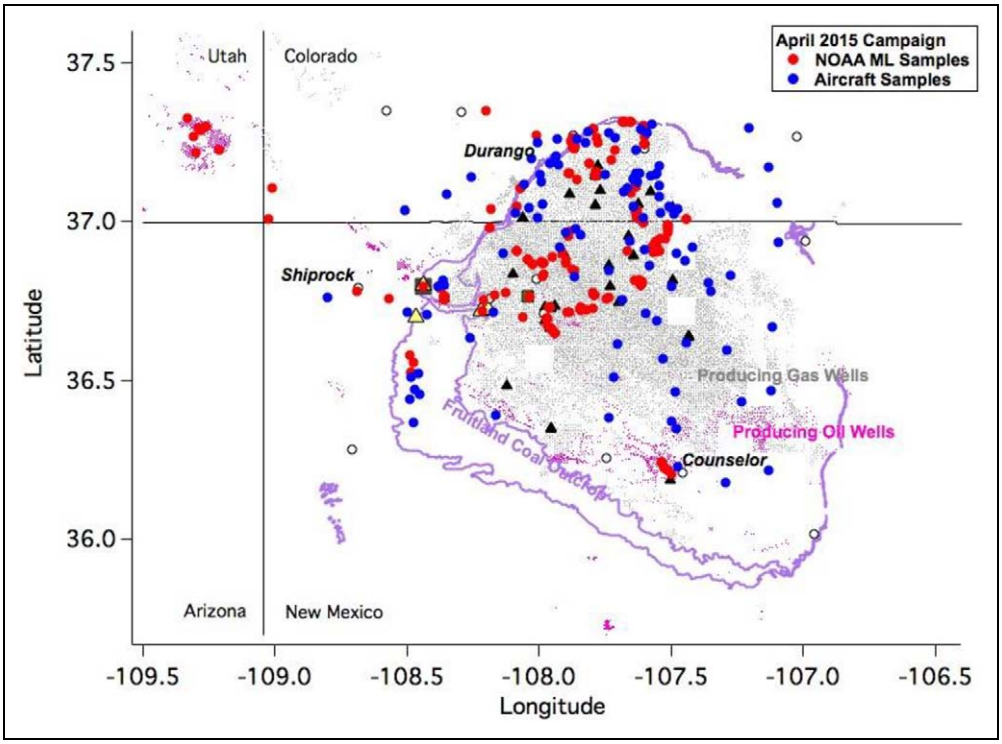

Figure 5. Map of flask air sampling locations for the NOAA Mobile Laboratory (ML, red circles) and the NOAA P-3 and SA Mooney aircraft (blue) during the April 2015 campaign. DOI: https://doi.org/10.1525/elementa.038.f5

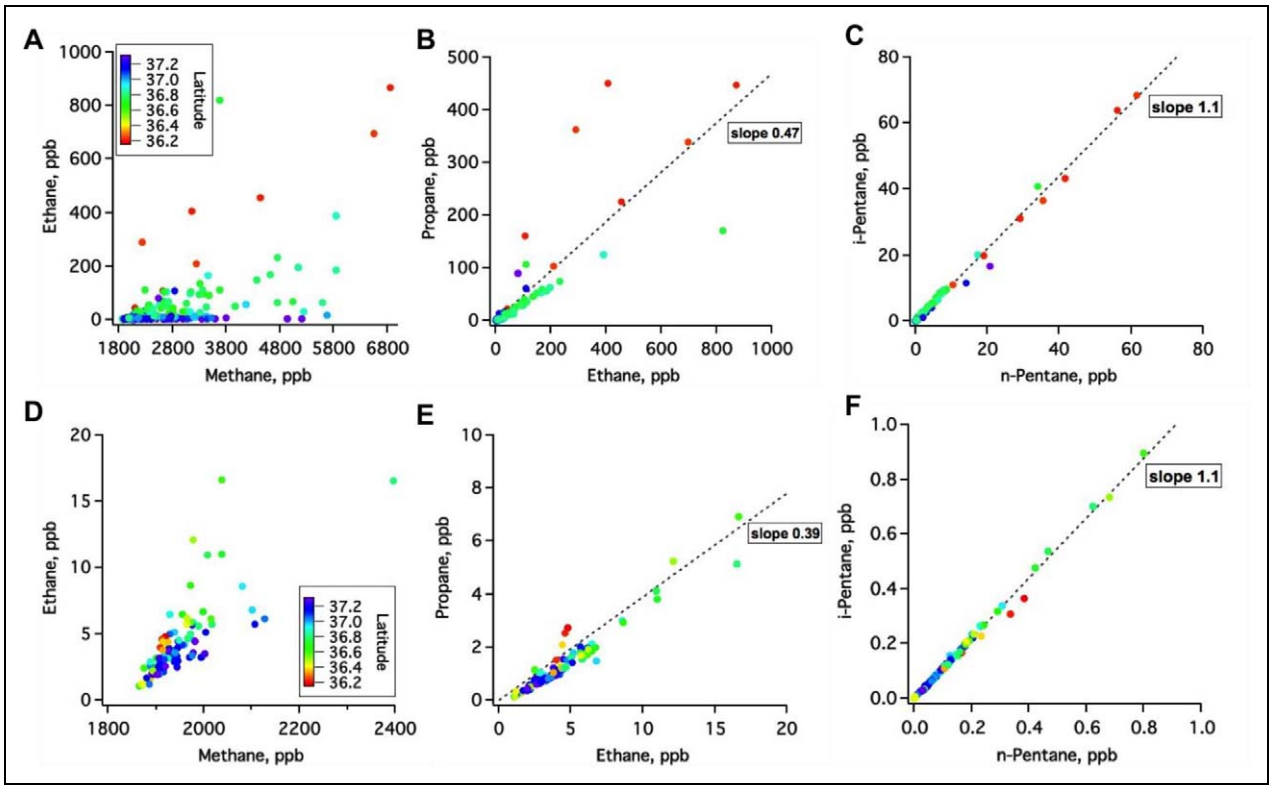

Figure 6. Correlation plots for C_2H_6-to-CH_4, C_3H_8-to-C_2H_6, and iC_5H_{12}-to-nC_5H_{12} in the ML (A to C) and aircraft (D to F) SJB discrete air samples in April 2015. DOI: https://doi.org/10.1525/elementa.038.f6

latitudes between 35.00N and 37.52N. During these flights, PBL horizontal winds were mostly from the West, which allowed us to attribute intercepted emission plumes to sources in Colorado for latitudes above the 37N State borderline and in New Mexico for latitudes below 37N.

Table 4. Date and time windows (local time) of Basin Survey flights in April 2015. DOI: https://doi.org/10.1525/elementa.038.t4

Aircraft	Date	Time window
SA Mooney		
	April 6	2:30 p.m. to 6:00 p.m.
	April 9	11:50 a.m. to 4:20 p.m.
	April 19	12:50 p.m. to 5:00 p.m.
	April 20	1:15 p.m. to 3:45 p.m.
	April 30	1:40 p.m. to 6:30 p.m.
NOAA P3		
	April 19	11 a.m. to 3 p.m.
	First survey	10:40 a.m. to 1:19 p.m.
	Second survey	1:20 p.m. to 3:30 p.m.

4.3.1. In situ CH_4 and C_2H_6 data analysis

Date and time windows for the SA Mooney and NOAA P-3 flights are listed in **Table 4**. Horizontal winds along the flight track were mainly from the West (see Mean Wind **Tables 5** and **6**), which is the typical flow in the region in the afternoon. Figures S16 and S17 show the flight track color-coded by CH_4 or C_2H_6 for each flight, as well as a C_2H_6 versus CH_4 correlation plot color-coded by latitude. Figure S18 shows a comparison of flask and in-situ CH_4 and C_2H_6.

Each survey flight consisted of several latitudinal transects, close to perpendicular to the mean horizontal wind direction in the PBL. Multiple CH_4 and C_2H_6 emission plumes were intercepted on each flight. The detected enhancements in an emission plume reflect the emission source composition and strength as well as atmospheric dispersion from the point source and the aircraft.

The mean horizontal wind speed in the PBL was lowest at 3.5 m/s on the April 9, 2015, flight. This flight had the largest range of enhancements for CH_4 and C_2H_6 of all survey flights. This was likely a combination of the early takeoff time (11:50 a.m. LT), the lower wind speed, and limited vertical dilution of the plume due to lower PBL height on that particular day (<1.5 km agl; Figure S4).

The flight mean horizontal wind speed (below 3,000 masl) was highest (10 m/s to 11 m/s) on April 6 and April 20, 2015. Measured CH_4 and C_2H_6 mixing ratios covered a wider range on April 20, 2015, than on April 6, 2015. The April 20 flight started earlier in the day than the April 6 flight, and the NLS and FMT data suggest the PBL was not fully grown until mid to late afternoon on April 2020. There is no wind profiler data for the April 6 flight.

All SA Mooney survey flights show multiple enhancements of CH_4 (up to ~ 300 ppb) and C_2H_6 (up to 35 ppb) above the local background levels in the PBL. These enhancements are detected in various locations over Colorado and New Mexico and sometimes on the edges of the SJB. C_2H_6 to CH_4 correlation plots for the survey flight in situ measurements show clusters of data along various

Table 5. CH_4 and C_2H_6 plume interval correlation statistics for the five SA Mooney survey flights. DOI: https://doi.org/10.1525/elementa.038.t5

	Colorado							New Mexico						
				Total Integrated Enhancement							Total Integrated Enhancement			
				CH_4 ppm.m		C_2H_6 ppb.m					CH_4 ppm.m		C_2H_6 ppb.m	
Date	Km	WS m/s	WD deg	$R^2 > 0.5$	$R^2 < 0.5$ or slope < 0.16%	$R^2 > 0.5$	$R^2 < 0.5$ or slope < 0.16%	Km	WS m/s	WD deg	$R^2 > 0.5$	$R^2 < 0.5$ or slope < 0.16%	$R^2 > 0.5$	$R^2 < 0.5$ or slope < 0.16%
April 6, 2015	375	10.1	228 ± 19	1.1	4.1	70	273	614	10.8	239 ± 19	1.9	3.2	300	473
April 9, 2015	326	3.5	225 ± 46	27.1	8.7	407	120	962	3.6	255 ± 31	52.5	23.0	2608	1019
April 19, 2015	334	8.0	261 ± 69	14.0	3.5	439	117	861	8.1	280 ± 21	32.8	5.5	2035	317
April 20, 2015	141	11.5	288 ± 20	0.8	0.9	54	57	570	10.8	291 ± 17	23.6	1.6	1248	102
April 30, 2015	313	6.9	256 ± 25	13.6	7.8	280	174	1084	6.3	286 ± 32	55.7	26.4	2301	974
Total	1,493 km			56.6	25.0	1249	741	4,091 km			166.6	59.7	8,492	2,885
Fraction of total integrated enhancement	CO			69%	31%	63%	37%	NM			74%	26%	75%	25%

Table 6. CH_4 and C_2H_6 plume interval correlation statistics for the three NOAA P3 survey flights on two different days with $R^2 > 0.5$ and slope > 0.16%. DOI: https://doi.org/10.1525/elementa.038.t6

	Colorado							New Mexico						
				Total Integrated Enhancement							Total Integrated Enhancement			
		Mean Wind		CH_4 ppm.m		C_2H_6 ppb.m			Mean Wind		CH_4 ppm.m		C_2H_6 ppb.m	
Date	Km	WS	WD	$R^2 >$ 0.5	$R^2 <$ 0.5	$R^2 >$ 0.5	$R^2 <$ 0.5	Km	WS	WD	$R^2 >$ 0.5	$R^2 <$ 0.5	$R^2 >$ 0.5	$R^2 <$ 0.5
March 24, 2015	410	5.7	287 ± 101	6.9	1.5	157	36	829	5.3	277 ± 61	18	6.1	1105	394
April 19, 2015 A	207	5.2	269 ± 53	19.3	1.3	396	25	732	3.9	261 ± 64	51	9.2	3110	382
April 19, 2015 B	128	7.9	285 ± 31	9.9	0.6	337	22	568	7.1	258 ± 19	18	2.4	925	148
Total	746			36.1	3.4	891	83	2129			88	18	5140	924
Fraction of integrated enhancement		CO		91%	9%	91%	9%		NM		83%	17%	85%	15%

correlation slopes, which depend strongly on latitude. Drier gas operation emission plume C_2H_6 to CH_4 slopes (0% to 5%) are observed over CO (>37N), while slopes over New Mexico range mostly between 3% and 10%.

The NOAA P-3 conducted two survey flights with very similar spatial patterns. On March 24, 2015, the flight concluded with 3 N-S transects on the E side of the SJB. On April 19, 2015, the aircraft completed one SJB survey from 10:40 a.m. to 1:19 p.m. (LT) and repeated the same survey over the SJB in the afternoon, leaving the region at 3:30 p.m. Figure S17 shows the NOAA P-3 flight data, separating the April 19, 2015, first and second basin surveys (A and B). The early flight on April 19, 2015, has a lower mean horizontal wind speed, and it exhibits the largest enhancements and a very clear latitudinal dependence of the C_2H_6 to CH_4 correlation slopes. The two nearly identical flight maps on April 19 show that the largest enhancements were detected in different locations, likely due to varying dispersion conditions and potentially time varying emissions.

Next, we explain the in situ CH_4 and C_2H_6 aircraft data analysis (see also SM Text Section 2.7 and Figure S19). We assume that the two aircraft data sets represent independent and representative sampling of the basin CH_4 emissions on a few days in spring 2015. Similarly to other studies, we attribute CH_4 emission plumes to different sources depending on whether C_2H_6 is co-emitted, as is expected for thermogenic gas sources (Smith et al., 2015; Mielke-Maday et al., 2019).

For each flight, we first derive PBL CH_4 and C_2H_6 enhancements by subtracting for each flight the observed minimum CH_4 and C_2H_6 PBL mixing ratios from the time series. To reduce the impact of high-frequency noise on the C_2H_6 in situ measurements and reduce the impact of different sampling frequencies and cell volumes for the two trace gas analyzers, we apply a 10-s running average to the CH_4 and C_2H_6 enhancement time series, noted ΔCH_4 and ΔC_2H_6 thereafter.

For data intervals between two successive smoothed ΔCH_4 local extrema (from a local minimum to a local maximum or from a local maximum to a local minimum), we calculate the integrated enhancements $i\Delta CH_4$ and $i\Delta C_2H_6$ along the flight path interval (ppb km). If the maximum ΔC_2H_6 in the interval is above 100 ppt, we compute the ΔC_2H_6 to ΔCH_4 correlation slope, *y*-axis intercept, and the associated coefficient of determination R^2.

For each SA Mooney flight, we find that between 102 and 156, ΔCH_4 and ΔC_2H_6 data intervals have $R^2 > 0.5$. The mean *y*-axis intercept for the correlation plots ranges between 43 ppt and 50 ppt, depending on the flight with a standard deviation between 26 ppt and 63 ppt. This suggests that our single PBL background correction for each flight to derive local enhancements and then interval correlation slopes is sufficient.

Finally, for each flight, we calculate the total integrated enhancements (TIE) for both ΔCH_4 and ΔC_2H_6 as the sum of all interval $i\Delta CH_4$ and $i\Delta C_2H_6$ with either $R^2 > 0.5$ or $R^2 < 0.5$, distinguishing geographically between the northern SJB and southern SJB flight intervals.

To separate different source contributions, we assume that if ΔCH_4 and ΔC_2H_6 in an interval have an $R^2 > 0.5$, the two gases are co-emitted by a nearby fossil fuel source or group of sources in the ratio of their observed correlation slope (similar to ground sampling results in Section 4.2).

Conversely, we assume that flight intervals with no C_2H_6 enhancements or with $R^2 < 0.5$ are contributed by CH_4 sources with no C_2H_6—such as the degassing sampled along the Fruitland coal outcrop in La Plata County and on SUIT land or by biogenic sources or by a mix of sources with different composition leading to poor correlation between CH_4 and C_2H_6.

Aggregated results for both aircraft enhancement data sets are in Tables 5 and 6. Our analysis shows that ~25% of the SJB detected CH_4 hot spot was located over Colorado. In April 2015, wells in Colorado produced 33% of the SJB gas and CBM production and represented 13.4% of active gas and CBM wells in the basin. Both data sets have ~75% of the total detected CH_4 anomaly and 85% of the total detected C_2H_6 anomaly located over New Mexico.

For both aircraft data sets, we identified over 600 plume segments with correlated CH_4 and C_2H_6 enhancements

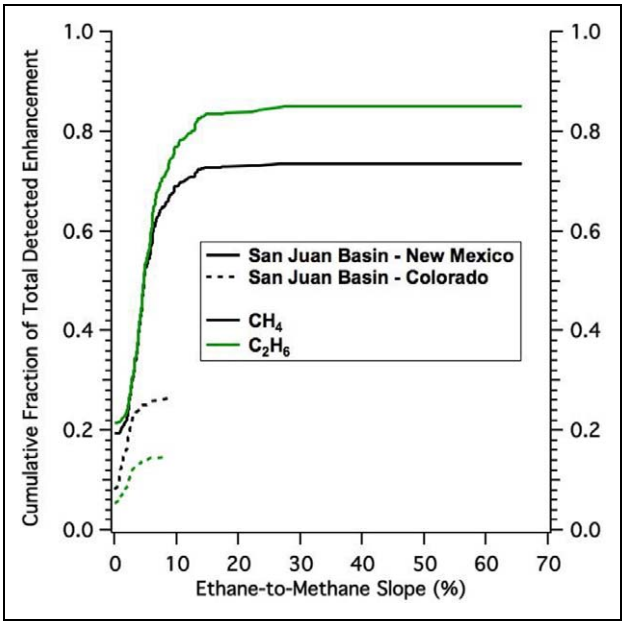

Figure 7. Cumulative fractions of the SJB CH_4 (black) and C_2H_6 (green) hot spots contributed by plumes with different C_2H_6 to CH_4 correlation slopes detected over Colorado (dashed lines) and New Mexico (continuous lines). The hot spot contribution calculation uses all plumes integrated enhancements derived for the five April 2015 SA Mooney flights. The sum of the NM and CO end points for each gas cumulative curves is equal to 1. DOI: https://doi.org/10.1525/elementa.038.f7

($R^2 > 0.5$). CH_4 and C_2H_6 enhancements were distributed all over the basin (Figures S20 and S21 for Mooney data only). As mentioned earlier, larger enhancements were observed on aerial PBL surveys before noon and when horizontal PBL winds were low ($\sim$<5 m/s). The latitudinal distribution of the CH_4 enhancements over the SJB is very similar to the downwind CH_4 plume measured by the NOAA Twin Otter on two flights (Figure S22). Ninety-five percent and ninety-eight percent of the observed CH_4 TIE for intervals with $R^2 > 0.5$ over New Mexico and Colorado, respectively, were due to intervals with at least 10 ppb gradients in CH_4.

We find that 72% to 85% of observed CH_4 and C_2H_6 TIE over the SJB were attributable to fossil fuel sources. For the Colorado portion of the basin, the aircraft data analysis results show that 69% to 91% of the observed CH_4 and C_2H_6 were attributable to fossil fuel sources.

If we use $R^2 > 0.75$ instead of $R^2 > 0.50$, the fractions of well-correlated enhancements are lower, and they explain 50% (63%) of the elevated CH_4 for the northern SJB and 58% (63%) for the southern SJB for the SA Mooney (NOAA P-3) flights.

Next, we look at the distribution of the relative contribution of intervals with different C_2H_6 to CH_4 correlation slopes to the detected CH_4 and C_2H_6 enhancements for the five SA Mooney flights combined (**Figure 7**). The curve origin at 0% slope is the TIE for intervals with either $R^2 <$ 0.5, or no C_2H_6 enhancement, or a ΔC_2H_6-to-ΔCH_4 slope less than 0.02%. We observed a much wider range of ΔC_2H_6-to-ΔCH_4 emission plume ratios over the southern SJB (0.50% to 66%) compared to the northern SJB (>0.1 to $\sim$9%), as was documented with ground observations (see Section 4.2). Further below, we use these ratios to separate contributions from natural gas, CBM, and oil operations in the southern SJB.

Table 7. NMHC correlation slopes for 101 air samples collected by aircraft over the San Juan Basin in April 2015. DOI: https://doi.org/10.1525/elementa.038.t7

Species	Slope (ppt/ppt)	R^2
C_3H_8 to C_2H_6	0.476 $\pm$ 0.014	1.0
iC_4H_{10} to C_2H_6	0.086 $\pm$ 0.003	1.0
nC_4H_{10} to C_2H_6	0.145 $\pm$ 0.006	0.99
iC_5H_{12} to C_2H_6	0.049 $\pm$ 0.002	0.98
nC_5H_{12} to C_2H_6	0.041 $\pm$ 0.002	0.98
nC_4H_{10} to iC_4H_{10}	1.68 $\pm$ 0.02	1.0
iC_5H_{12} to nC_5H_{12}	1.18 $\pm$ 0.02	1.0
C_6H_6 to nC_6H_{14}	0.21 $\pm$ 0.02	0.60

Finally, we investigate how the aircraft data analysis results are affected by flight time. We use the TIE results for six 1-h time windows between noon and 6 p.m. LT, merging all five SA Mooney flights. It is important to note that the basin coverage varies for each hourly interval. The median fraction of CH_4 TIE with $R^2 > 0.5$ and a ΔC_2H_6-to-ΔCH_4 slope >0.02% is 68% over Colorado and 76% over New Mexico, which is in good agreement with the time aggregated Mooney flight results we have presented above. Minimum and maximum hourly fractions are shown in Table S7.

4.3.2. NMHC in aircraft flasks and NMHC TD emission estimates

Oil, NG, and CBM operations in the SJB are known to be a significant source of ozone precursor emissions (Parikh et al., 2017a). Our flask measurements in gas plumes showed that when both CH_4 and C_2H_6 were enhanced, measured $C_{3\text{-}5}$ alkanes were also elevated and well correlated. We conclude that the bulk of the measured C_2-C_5 alkanes are very likely co-emitted with uniform ratios throughout the basin (**Figure 6**, Panels D to F). **Table 7** gives a summary of NMHC correlation slopes calculated for the SJB aircraft flask data by orthogonal difference regression, assuming a 10% relative uncertainty on all NMHC measurements.

Here, we also derive TD emission estimates for the measured C_2-C_5 alkanes. We first scale the average, low, and high aircraft mass-balance estimates of total CH_4 emissions from Smith et al. (2017) using the ratio of C_2H_6 TIE to CH_4 TIE for the five SA Mooney flights. We obtain three emission scenarios: mean, low, and high. The mean basin-scale emission estimate for C_2H_6 is 5.0 $\pm$ 1.9 tonnes/h, with a low–high range of 2.9 to 7.8 tonnes/h (**Table 8**).

Table 8. Top-down estimated emissions (tonnes/h) for measured NMHC in the SJB. DOI: https://doi.org/10.1525/elementa.038.t8

Species	Mean Estimated Emissions tonnes/h	Low–High Emission Range tonnes/h
CH_4[a]	62 ± 23	35 to 96
C_2H_6	5.0 ± 1.9	2.9 to 7.8
C_3H_8	3.5 ± 1.3	2.0 to 5.4
iC_4H_{10}	0.8 ± 0.3	0.5 to 1.3
nC_4H_{10}	1.4 ± 0.5	0.8 to 2.2
iC_5H_{12}	0.6 ± 0.2	0.3 to 0.9
nC_5H_{12}	0.5 ± 0.2	0.3 to 0.8
C_3-C_5 total	6.8 ± 2.5	3.9 to 10.6

[a]Based on Smith et al. (2017).

To derive emission estimates for the other NMHC, the C_2H_6 flux estimates are scaled by the aircraft samples measurement correlation slopes reported in **Table 7**. The mean basin-scale emission estimate for the measured C_3-C_5 alkanes is 6.8 ± 2.5 tonnes/h, with a low–high range of 3.9 to 10.6 tonnes/h (**Table 8**).

Our mean emission estimates for C_3-C_5 adds up to three fourth of the WESTAR inventory total VOC emission estimate of 9.3 tonnes /h (Parikh et al., 2017a, 2017b). Our estimate does not include all VOCs emitted by O&G sources such as higher alkanes and methanol. The WESTAR SJB inventory data publically available do not contain a breakdown of VOC emissions by species, which limits the interpretation of our finding. The WESTAR inventory has 90% of O&G total VOC emissions in the SJB attributed to operations in New Mexico (Parikh et al., 2017b). This is close to the 85% New Mexico versus 15% Colorado partitioning we derived for the SJB C_2H_6 anomaly detected by aircraft in spring 2015.

The emission estimates for C_2H_6 in the SJB are similar in magnitude to emissions from dry gas producing basins reported by Peischl et al. (2018). The emission estimates for C_3-C_5 NMHCs for the SJB are significantly lower than the 25.4 ± 8.2 tonnes/h reported by Pétron et al. (2014) for the Denver Basin, which produces oil, liquid condensate, and wet gas in NE Colorado.

4.3.3. San Juan Basin methane emission attribution

In this section, we use the aircraft CH_4 to C_2H_6 interval analysis results to quantify relative contributions from different CH_4 sources to the hot spot detected by aircraft.

In the vicinity of the San Juan underground coalmine in NM, the SA Mooney detected 16 plume intervals on five different flights with C_2H_6-to-CH_4 correlation slopes ranging between 0.8% and 1.5% (compared to 0.9% for ground flasks collected in the air shaft emission plume on June 14, 2015). These plumes contributed to 2% of the SA Mooney total CH_4 TIE for NM. The NOAA P-3 detected a plume on each survey in the vicinity of the San Juan coalmine, and these plumes contributed 1.4% of the NOAA P-3 total CH_4 TIE for NM.

We postulate that plume intervals with correlated C_2H_6 and CH_4 ($R^2 > 0.5$) and a C_2H_6-to-CH_4 slope between 0.16% and 10%—and not attributed to the San Juan coalmine—are attributable to NG or CBM operations in CO or NM. The iΔCH_4-weighted mean ΔC_2H_6 to ΔCH_4 correlation slope for these plumes is 2.3% (2.7%) in the northern SJB and 4.6% (4.4%) for the southern SJB in the SA Mooney (NOAA P-3) data set. This reflects the larger fraction of dry gas and CBM production in Colorado. Our analysis shows that 66% (SA Mooney) to 75% (NOAA P-3) of the detected CH_4 enhancements fall in the NG and CBM category. **Table 9** and **Figure 8** summarize the source attribution results discussed below.

The U.S. Geological Survey reports that most coal beds in the SJB Fruitland formation will produce thermogenic CH_4 that can be wet or dry (Ridgley et al., 2013). Therefore, some CBM wells in the basin produce very dry gas with no detectable C_2H_6. CH_4 emissions or gas vented from these wells will not show co-emitted C_2H_6 and will show up in the "Other category." This means that 66% is likely a lower bound estimate of the NG and CBM operations combined contribution to the observed SJB CH_4 hot spot.

Wetter gas (with larger fraction of C_2-C_5 relative to C_1-C_5) is often a sign of a less mature hydrocarbon reservoir with natural gas liquids coproduced with CH_4. We postulate that plumes with >10% slopes are due to emissions from condensate or oil and associated gas operations. Only in New Mexico did the aircraft detect plumes with correlated C_2H_6 and CH_4 and slopes >10%. These plumes represented 8% of CH_4 TIE and 13% of C_2H_6 TIE for New Mexico and ~ 6% of the CH_4 TIE for the entire basin.

Oil production in the SJB increased from an average of $7.2x10^3$ bbl/day over the 2003 to 2009 period to 23.9 × 10^3 bbl/day in April 2015. This last figure represented 6% and 0.25% of the State and U.S. total oil production volumes, respectively. Over this period, NG and CBM production in the basin decreased by 34%. In 2019, mean daily production statistics for the basin were lower for oil (−4%), natural gas (−8%), and CBM (−26%) compared to the April 2015 numbers.

The annualized TD mean estimates for the SJB total CH_4 emissions for 2003 to 2009 and April 2015 are similar (Kort et al., 2014; Smith et al., 2017). However, there is no attribution for the early period and for recent years. A better understanding of emission magnitudes and trends for the SJB and other basins would require long-term BU and TD emission quantification and attribution studies.

Based on what has been reported so far, CH_4 seepage from the Fruitland coal outcrop could only occur over Colorado. Based on our surface air sampling in outcrop seepage gas plumes, we postulate that outcrop gas has not co-emitted C_2H_6. Emission plumes with no C_2H_6-to-CH_4 enhancement correlation detected over Colorado were categorized as "CO coal outcrop and Other." Our analysis shows that CH_4 enhancements detected over Colorado and with no correlated C_2H_6 or a C_2H_6-to-CH_4 correlation slope <0.16% represented a smaller fraction

Table 9. Source attribution for the SJB CH_4 BU emission estimates and for the CH_4 hot spot detected by aircraft in April 2015. DOI: https://doi.org/10.1525/elementa.038.t9

	Attribution (%)					
	Bottom-Up Emissions		SA Mooney Enhancements		NOAA P-3 Enhancements	
Sources	Colorado	New Mexico	Colorado	New Mexico	Colorado	New Mexico
NG + CBM	13	51	18	48	25	53
Associated gas/oil	–	1.6	–	4.5	–	6
Coal	–	7	–	1.5	–	1.0
Outcrop	24	–	8	–	2.3	–
Other	2.5	1.5		19		12

Note that the "Outcrop" and "Other" sources are lumped for the aircraft data over Colorado. Note that due to rounding, the total for each category (BU, SA Mooney and NOAA P-3) does not add up to exactly 100.

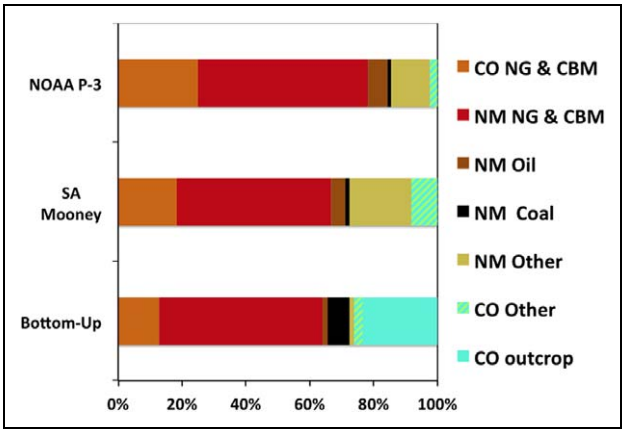

Figure 8. Source contribution breakdown for the SJB CH_4 bottom-up emission estimates (bottom bar, see **Table 1**) and the SJB CH_4 hot spot detected by aircraft in April 2015: SA Mooney (middle bar) and NOAA P-3 (top bar). New Mexico (NM) and Colorado (CO) contributions are shown separately. The aircraft data analysis could not further differentiate the origin for CH_4 enhancements with no correlated C_2H_6. As a result, contributions to the aircraft detected hot spot breakdown over CO from outcrop seepage and undetermined sources are lumped in "CO Other." CBM and NG stand for coal bed methane and natural gas, respectively. DOI: https://doi.org/10.1525/elementa.038.f8

of the total CH_4 TIE: 8% for SA Mooney data and 2% for the NOAA P-3 data.

We conclude that degassing from the outcrop contributed at most between 2% and 8% of the CH_4 hot spot observed by the two aircraft. This finding agrees with Smith et al. (2017). Based on flights targeting emission plumes from known outcrop vents SW of Durango, they argued that these sources "are a small fraction of the basin total," ranging from 0.02 to 0.12 Tg CH_4 yr^{-1}.

The Colorado outcrop emission contribution to the detected CH_4 hot spot is much smaller than the 24% BU emission estimates suggest (**Table 9**). However, outcrop degassing field results have been shown to be variable from year to year (LTE, 2017). Current outcrop gas seepage emission estimates relying on spatially and temporally extrapolated field data likely carry very large uncertainties.

4.3.4. San Juan Basin natural gas and coal bed methane CH_4 emissions and infrastructure loss rates

Here, we use mean, low, and high total CH_4 emission scenarios based on results from Smith et al. (2017) and the aircraft data attribution results (**Table 9**) to derive mean, low, and high CH_4 emission estimates for NG + CBM and oil systems (**Table 10**). Mean estimates for both aircraft data sets are between 11 and 15 tonnes/h for Colorado and close to 30 tonnes/hr for New Mexico for NG + CBM systems and are 2.8 tonnes/hr to 3.9 tonnes/hr for oil operations in NM. The mean estimates we derive for total CH_4 emissions from oil, NG, and CBM operations in the SJB are 44.7 tonnes/h (Mooney) and 53.2 tonnes/h (P-3). These estimates are based on the analysis of in situ data from a few flights in spring 2015.

For comparison, the WESTAR 2014 SJB annual emission inventory equates to 42.5 CH_4 tonnes/h, assuming a constant emission rate (Parikh et al., 2017b). Note that Parikh et al. (2017a) warn that the SJB annual CH_4 emission estimate may be biased low due to missing or inadequate input data. The authors acknowledge that they did not include GHG for point sources with unknown Source Classification Code. Also, the inventory does not include CH_4 emissions for nonpoint O&G sources in CO due to the absence of a breakdown of GHG emissions by gas in a CDPHE emission inventory used as input. Finally, the inventory authors assumed a default control efficiency of 98% and a default capture efficiency of 100% for emission sources controlled by flares, for example, tanks, casing-head gas, and dehydrators, which is likely a best-case scenario.

The SJB total gas output was $\sim 8 \times 10^7$ m^3/day in April 2015. We use a 90% to 99% range for the produced NG or CBM CH_4 content in the SJB. Assuming a molar volume for the produced gas of 23.6 L per mole (pressure = 14.73 psi and temperature = 60°F), we derive mean (low–high) CH_4 loss rates for the SJB combined NG and CBM operations of

Table 10. Summary statistics for CH_4 BU emissions, PBL CH_4 enhancements, and CH_4 loss rates for the SJB. DOI: https://doi.org/10.1525/elementa.038.t10

	SJB CH_4 Attribution					
	Colorado			New Mexico		
Categories	**Bottom-Up**	**SA Mooney**	**NOAA P-3**	**Bottom-Up**	**SA Mooney**	**NOAA P-3**
Fraction of basin CH_4 TIE (%)	38.8	26.5	27.2	61.2	73.5	72.8
Fraction of CO or NM CH_4 emissions or TIE attributed to (%)						
NG + CBM[a]	32.9	69.3	91.5	83.8	65.5	73.3
Oil	—	—	—	2.6	6.1	8.5
Underground coal mine	—	—	—	11.3	2	1.5
Total for fossil fuel systems	32.9	69.3	91.5	97.7	73.6	83.3
Weighted average NG + CBM C_2H_6-to-CH_4 slope[a] (%)	—	2.3	2.7	—	4.6	4.4
Mean (low–high) CH_4 emissions attributable to NG+CBM systems[a,b] (tonnes/h)	7.6	11.3 (6.5 to 17.6)	15.3 (8.8 to 23.9)	30.5	29.7 (17 to 46.2)	32.9 (18.9 to 51.2)
Mean NG + CBM system CH_4 loss rate[b,c] (emissions/production in %) (low–high)	1.0 to 1.1	1.6 to 1.7 (0.9 to 2.7)	2.2 to 2.4 (1.4 to 3.8)	2.2 to 2.4	2.0 to 2.1 (1.1 to 3.4)	2.2 to 2.4 (1.3 to 3.8)

[a]Only plumes with 0.16% < C_2H_6-to-CH_4 slope < 10%.

[b]Removing the San Juan coal mine contributions.

[c]Assuming produced NG is 90% or 99% CH_4 and using low/high CH_4 emission scenario.

1.6% to 2.4% (0.9% to 3.8%) in Colorado and 2.0% to 2.4% (1.1% to 3.8%) in New Mexico during the field study for both aircraft data sets (**Table 10**).

These leak rates are similar to the 2015 national average estimates based on the EPA GHGI (1.4%) and on Alvarez et al. (2018; 2.3%). They are also comparable to TD results from other U.S. onshore O&G basins studied in 2015 (**Figure 5** in Peischl et al., 2018).

5. Discussion

The detection of locally or regionally elevated XCH_4 with aerial or satellite remote sensing can help identify strong sources, especially if (1) emissions persist over days to weeks (Thompson et al, 2016; Pandey et al., 2019; Varon et al., 2019; Cusworth et al., 2020), several months (de Gouw et al., 2020), or several years (Kort et al., 2014; Schneising et al., 2014; Shim et al., 2018), (2) emissions tend to accumulate at the surface (under strong temperature inversions, e.g., de Gouw et al., 2020) or show distinct plumes (Frankenberg et al., 2016), (3) sources are spatially separated (Cusworth et al., 2018), and (4) the area is well observed from space resulting in sufficient "good" data coverage (high albedo, low cloud, low aerosols, etc., all parts of data quality filters defined for each remote sensor and retrieval data product; de Gouw et al., 2020). It is important to recognize that the improved spatial coverage offered by remote sensing products can hide some of the complexity, biases, and total uncertainty attached to column retrievals, potentially affecting the data analysis and interpretation (Zhang et al., 2017; Varon et al., 2018; see more below).

In our paper, we use the 2015 campaign in situ aircraft data for CH_4 and C_2H_6 to attribute a mean total CH_4 emissions estimate derived from flights in April 2015 (Smith et al., 2017) to different sources. This allows us to estimate emissions for O&G sources and to calculate a mean CH_4 loss rate for CBM and natural gas operations for the time of the campaign.

We are not able to conduct a comparison of the SJB April 2015 CH_4 hot spot attribution with the earlier study by Kort et al. (2014), which looked at total basin-wide emissions. Given the large year-to-year variability in the reported surface chamber CH_4 flux measurements of the Fruitland coal outcrop surface degassing in La Plata County, we cannot estimate accurate outcrop mean emissions over 2003 to 2009. Also, we do not have TD constraints to quantify O&G CH_4 emissions separately for that earlier time period either.

The main difference between the earlier study and our paper lies in our effort to use a suite of long-term and campaign mode measurements to explain the different factors leading to the SJB CH_4 pollution as observed at the surface with instrumented vehicles, in the PBL with aircraft, and in the total air column by satellite. The region has strong local sources, emissions trapping due to topography, and wind patterns at night and pristine surrounding mountains. The basin is expected to stand out as an XCH_4 local anomaly, but it should not be the only one, as noted further below.

All U.S. O&G basins our team has visited in the last decade have much higher CH_4 levels at the surface at

night and early morning under low wind conditions. The accumulated pollution from nocturnal emissions will dilute vertically as the boundary layer grows and then be flushed out of the region. This flushing happens sooner over a flat terrain than in a topographical basin like the SJB—which also has downslope surface winds at night that carry emission plumes E/SE (see illustrations in supplementary material Figure S23). Below, we use a simple calculation to translate a typically observed nighttime CH_4 surface air anomaly into an early and midmorning vertical column mean enhancement.

The vertical sensitivity of the SCIAMACHY CH_4 column retrievals from nadir shortwave infrared radiation spectra—for cloud free pixels—mostly follows the air pressure down to the surface for solar zenith angles <70° (Buchwitz et al., 2005; Frankenberg et al., 2006). Therefore, the SCIAMACHY retrievals should be a reasonable estimate of CH_4 air column mixing ratio averages. The total column retrievals should be insensitive to the height of the PBL. Any vertical mixing of CH_4-rich surface air without horizontal dispersion will not change the column average mixing ratio over a location.

With a midmorning overpass time (10:40 a.m. $\pm$ 40 min LST), the SCIAMACHY satellite detected columns with enriched CH_4 near the surface, resulting from the accumulation of overnight and early morning emissions. A simple calculation shows that it takes a 4-ppm CH_4 enhancement in a 100 m surface layer ($\sim 1\%$ of the atmosphere column over the SJB in pressure) to create a 40 ppb total atmospheric column XCH_4 enhancement above the local background column. This is very close to the largest mean column anomaly depicted in the local anomaly map by Kort et al. (2014). As shown in Section 4.2.2, 2 ppm to 4 ppm surface air CH_4 large-scale enhancements were detected in the SJB by the NOAA and CU INSTAAR vans at night and early morning before the onset of the PBL growth and surface air dilution with cleaner air from above entrainment.

The 2 ppm to 4 ppm surface air enhancements reflect the accumulation of local emissions under nocturnal and early morning low surface air dispersion conditions. Our analysis of wind regimes over the SJB implies that on most days, the SCIAMACHY satellite midmorning overpass time occurs before the nightly CH_4 emissions buildup in the basin has been flushed away. In other words, the satellite likely scanned the region's atmosphere close to when the PBL CH_4 pollution peaks and when the basin's airshed stands in stark contrast with "cleaner" air columns over nearby remote (source-free) and high-elevation terrain.

The mean TD CH_4 emission estimate reported by Smith et al. (2017) for the SJB is 62 $\pm$ 23 tonnes/h. This is of similar magnitude as aircraft mass balance estimates derived for other U.S. O&G producing regions: the Barnett Shale, TX (66 $\pm$ 22 tonnes/h; Peischl et al., 2018), the Uinta Basin, UT, (55 $\pm$ 15 tonnes/h; Karion et al., 2013), and the Haynesville Shale, LA, and TX (51 $\pm$ 16 tonnes/h; Peischl et al., 2018). Only the Barnett was a mature shale gas formation in the United States by 2009. The Uinta Basin in NE Utah has been producing natural gas for decades. These two regions did not show up as hot spots on the Kort et al. (2014) 2003 to 2009 local anomaly map.

The SJB TD CH_4 emission estimate is also less than half of an inverse model emission estimate for the SJV, CA (Jeong et al., 2016), where dairy livestock is the largest CH_4 source. The southern SJV appears as a smaller CH_4 hot spot than the SJB on the Kort et al. anomaly map. This may be the result of the nocturnal surface CH_4 emission buildup dispersing more effectively by midmorning in the SJV than in the SJB.

A detailed analysis of the various potential factors impacting the detectability of known large CH_4 source regions in different satellite data products would be quite valuable, but (1) it is beyond the scope of this paper and (2) a study team with satellite data experts would better accomplish it.

In the SJB, most afternoons, stronger wind speeds and a deeper PBL acted in concert to reduce the CH_4 pollution levels detected with the instrumented vans near the surface or with the aircraft in the PBL (Figures 2, 4, and S4). A satellite instrument with the same sensitivity as SCIAMACHY, but with a mid to late afternoon overpass time, may not have detected such a large and persistent CH_4 hot spot over the SJB.

The SJB does not stand out as a regional anomaly in a more recent map of TROPOMI (TROPOspheric Monitoring Instrument) retrievals of XCH_4 over the United States for December 2018 to March 2019 (**Figure 1** in de Gouw et al., 2020). This may partly be due to the very limited number of valid retrievals for large portions of the Rocky Mountains during the entire period (Figure S1 in de Gouw et al., 2020). The authors explain that cloud cover, low surface albedo, higher topography, and other factors can affect the retrieved CH_4 data quality. Despite a 1:30 p.m. LT TROPOMI overpass time, de Gouw et al. (2020) note the largest enhancement detected in another U.S. oil and natural gas basin, the Uinta Basin in NE Utah, occurred "over the deepest parts of the Basin, consistent with the accumulation of emissions underneath inversions," a phenomena reported by earlier studies focused on explaining the basin's wintertime surface ozone pollution (Schnell et al., 2009; Oltmans et al., 2014).

A reliable GHG emission monitoring system cannot rely exclusively on remote sensing products (Cusworth et al., 2018; Nisbet et al., 2020). Remote sensing instruments can have radiometers calibrated for radiance, but the quantity of interest is the in situ profile of the dry air mole fraction of CH_4. The latter is estimated by a radiative transfer model, which has to incorporate several assumptions about the atmosphere and the surface. It remains a fundamental weakness of remote sensing that GHG atmospheric column retrievals cannot be calibrated. GHG retrievals can only be compared to relatively sparse and never entirely coincident calibrated in situ measurements or evaluated against ground-based remote sensing data products (Wunch et al., 2010, 2011; Geibel et al., 2012; Buchwitz et al., 2015; Loew et al., 2017).

Atmospheric column gradients are affected by emission strength and distributions, air dispersion, and changes in surface elevation. Satellite retrievals based on

shortwave infrared radiation can show XCH_4 and XCO_2 gradients related to localized emissions, but retrievals can also be affected by other spatially variable factors such as water vapor, clouds, aerosols, and surface reflectivity (Buchwitz et al., 2005; Frankenberg et al., 2006, 2008).

The "translation" of atmospheric GHG in situ measurements or remote sensing retrievals into emission estimates or emission trends for a given region and time period requires careful analysis of the data quality and data representativeness as well as advanced and validated surface flux estimation and attribution methods. Coordinated research and operational data collection are necessary to further refine and compare emission detection, estimation, and attribution methods at various scales.

Vaughn et al. (2018) showed the importance of perfect overlap in time and space of emission estimation efforts to successfully compare temporally varying CH_4 emission for the Fayetteville dry shale gas basin in Arkansas in fall 2015. The authors compared midday spatially resolved emission estimates based on aircraft measurements and concurrent facility-level measurement and operational data. The coordinated research in that particular basin revealed the large contribution of daytime gas venting practices for liquid unloading at well pads to midday basin total CH_4 emissions. A follow-up coordinated pilot study evaluated the potential of CH_4 emission detection and cost-effectiveness of two airborne techniques against the traditional ground-based leak detection and repair method (Schwietzke et al., 2018).

Other coordinated studies in one particular basin (San Juan Basin; Frankenberg et al., 2016; Smith et al., 2017; Barnett Shale, TX; Zavala Araiza et al., 2015), or spread over different U.S. O&G basins (Alvarez et al., 2018), have brought many useful insights on source processes and emission distributions. Field measurements on-site, downwind of facilities, and from the air have demonstrated how anomalously large emitters contribute a substantial fraction of total O&G emissions in a producing region as well as for each natural gas supply chain segment.

Some independent studies using different atmospheric CH_4 observations or retrievals and emission quantification techniques have shown substantial disagreement between estimates of O&G emission trends over the United States (Bruhwiler et al., 2018; Lan et al., 2016; Turner et al., 2016) or over a specific Basin (Schneising et al., 2014; Peischl et al., 2016).

Here, we have shown that in situ multiple species measurements can be used to characterize CH_4 emission plumes and attribute basin CH_4 emissions to different sources. In situ meteorological and trace-gas measurements throughout the region and at different times of the day offered a more complete picture of the SJB CH_4 sources and hot spot dynamics than previously reported. In terms of CH_4 emissions and loss rate for NG and CBM operations, TD estimates for the region did not stand out from other U.S. O&G basins and were in line with Alvarez et al.'s (2018) mean results for the United States in 2015.

Before concluding this paper, we want to note that field operations and emissions captured during the campaign may not be representative of typical or annual conditions in the SJB. Some O&G activity levels can vary in response to multiple independent factors. The study authors and other researchers, who were in the field during the April 2015 campaign, noticed a more visible presence of O&G technicians in charge of checking site operations and servicing equipment. Reliable and effective O&G sources management, leak detection and repair (LDAR), and malfunction or leak prevention are critical components of emissions mitigation. It is possible that emissions mitigation from increased site visits was enhanced during the campaign. Continuous emissions monitoring systems for operators and more frequent remote sensing and in situ observations for independent emissions quantification will support stronger mitigation and policy-making.

6. Conclusions

For several years, nongovernmental organizations, industry, universities, local, and federal government entities in the United States have partnered to advance anthropogenic CH_4 emission quantification methods and mitigation assessments, especially from the natural gas sector (ICF, 2016; Alvarez et al., 2018; Schwietzke et al., 2018).

Our study has focused on improving the scientific understanding of CH_4 emissions in a fossil fuel rich basin in the southwestern United States, the San Juan Basin, close to the U.S. Four Corners. This region had become known as the U.S. largest local CH_4 anomaly or hot spot based on the analysis of SCIAMACHY satellite XCH_4 retrievals between 2003 and 2009 by Kort et al. (2014).

We provide a breakdown of source contributions to the SJB CH_4 hot spot detected by two aircraft equipped with fast in situ CH_4 and C_2H_6 measurements in April 2015. Extensive O&G and CBM operations throughout the SJB contributed at least 66% to 75%, while gas seepage from the Fruitland coal outcrop in La Plata County, CO, contributed 2% to 8% at most. Seventy-five percent (85%) of CH_4 (C_2H_6) total enhancements over the local background air was detected over New Mexico. Oil operations in New Mexico only contributed 5% to 6% of the detected CH_4 anomaly.

The SJB, similar to other topographical basins with local sources, experiences aggravated surface air CH_4 (and NMHC in the southern SJB) pollution as surface emissions accumulate under low wind and during surface temperature inversion at night and until midmorning. The SCIAMACHY satellite captured this atmospheric CH_4 overnight buildup during its midmorning overpass. It takes 4 to 6 h for the typical afternoon westerly winds to flush the CH_4 (and any co-emitted gases) pollution buildup outside of the basin. This nocturnal and early morning enhanced surface air hydrocarbon pollution due to emissions in O&G basins deserves more scrutiny, especially the investigation of potentially repeated exposure to elevated air toxic levels among local residents and industry workers (Mielke-Maday et al., 2019).

The mean leak rate estimates for CBM and natural gas operations in the SJB in April 2015 are 1.6% to 2.4% in Colorado and 2.0% to 2.4% in New Mexico (Table 10, Section 4.3.4). These numbers are in line with TD and BU estimates from other U.S. O&G basins. This implies

that the SJB is not the largest U.S. CH_4 anomaly in terms of O&G emissions or leak rate. However, the impact of these sources on the basin airshed can be amplified by the local topography and meteorology.

A more detailed assessment of fossil fuel production sources and emissions on the SJB air quality would require process-level emission studies, similar to other studies that have unfortunately almost exclusively focused on CH_4 so far (Allen et al., 2013; Alvarez et al., 2018; Vaughn et al., 2018; Zaimes et al., 2019). The SJB, having been a major producer of gas and CBM for decades, is home to a large number of older producing wells. It may be insightful to characterize emissions for facilities of different sizes, types, and ages to better estimate current and potential future hydrocarbon emissions from this large and complex source sector.

This work and previous studies have shown the intrinsic value of coordinated research and operational data collection to compare and refine CH_4 emission detection, estimation, and attribution methods at various scales. At this critical time in the planet and human history, reliable, comprehensive, and up-to-date GHG emission estimates by source type and at scales relevant for policy-making are still lacking. However, as much as accurate GHG emission estimates are valuable, even more time critical is the need for "rapid and deep" mitigation, in other words much bolder emission cuts necessitating substantial societal and industry transformations, to meet the Paris Climate Agreement goals (Nisbet et al., 2019, 2020; Anderson et al., 2020).

Authors' note

Any opinion, findings, and conclusions or recommendations expressed in this paper are those of the authors and do not necessarily reflect the views of the project participants and sponsors.

Data Accessibility Statement

Surface meteorological data for monitoring stations in the San Juan Basin are archived in the EPA Air Quality System Data Mart and can be accessed via links provided here: https://www.epa.gov/outdoor-air-quality-data.

NOAA P-3 data from the SONGNEX campaign are accessible via Data menu at: https://www.esrl.noaa.gov/csd/projects/songnex/.

NOAA GML in situ and flask multiple species data can be requested from the corresponding author.

Supplemental files

The supplemental files for this article can be found as follows:

Text S1. Contains Tables S1 to S7, Figures S1 to S23, Supplementary Text. Docx.

Acknowledgments

The authors thank local authorities and staff members for their support for the field campaign. The New Mexico Environment Department coordinated planning discussion and outreach events for the multiagency project and provided site and power access for the NOAA wind profilers at the FMT and NLS locations. The Southern Ute Indian Tribe Environmental Programs Division provided site and power access for the Leosphere wind profiler at the Ute 1 location. The Southern Ute Indian Tribe Environmental Programs Division and Department of Energy and the Navajo Nation Environmental Protection Agency provided escort and shared technical expertise. The Bureau of Land Management Farmington office lent the five ground measurement team members personal air safety monitors (H_2S and CO). The authors also thank the reviewers and editors for their valuable suggestions.

Funding information

This research project was supported in part by the NOAA Climate Program Office, the NOAA Atmospheric Chemistry, Carbon Cycle, and Climate Program under Grant No. NA14OAR0110139, as well as the AirWaterGas Sustainability Research Network funded by the National Science Foundation under Grant No. CBET-1240584. We acknowledge funding from the Bureau of Land Management through an Inter Agency Agreement with the National Oceanic and Administration for aircraft and wind LIDAR research support.

Author contributions

- Contributed to conception and design: GP, BM, BV, JK, ET, IM-M, O-S, SS, SC, JP, CS, AW, PT, RS.
- Contributed to acquisition of data: GP, BM, ET, BV, JK, IM-M, OS, BH, SS, SC, JP, PL, EM, MC, AC, CS, CS, TN, SW, CK, TC, MR, BV, RS.
- Contributed to analysis and interpretation of data: GP, BM, BV, IM-M, OW, ED, BH, SS, LB, BV, PT.
- Drafted and/or revised the article: GP, BV, ED, SS, JP, PT, RS, BM, BH, MC.
- Approved the submitted version for publication: GP, BM, BV, ET, JK, IM-M, OS, ED, BH, SS, SC, JP, PL, EM, MC, AC, CS, TN, SW, DK, LB, CK, TC, AW, MR, PT, RS.

References

Allen, DT, Pacsi, AP, Sullivan, DW, Zavala-Araiza, D, Matthew Harrison, M, Keen, K, Fraser, MP, Hill, AD, Sawyer, RF, Seinfeld, JH. 2015a. Methane emissions from process equipment at natural gas production sites in the United States: Pneumatic controllers. *Environ Sci Technol* **49**(1): 633–640. DOI: http://dx.doi.org/10.1021/es5040156.

Allen, DT, Sullivan, DW, Zavala-Araiza, D, Pacsi, AP, Harrison, M, Keen, K, Fraser, M, Hill, AD, Lamb, BK, Sawyer, RF, Seinfeld, JH. 2015b. Methane emissions from process equipment at natural gas production sites in the United States: Liquid unloadings. *Environ Sci Technol* **49**(1): 641–648. DOI: http://dx.doi.org/10.1021/es504016r.

Allen, DT, Torres, VM, Thomas, J, Sullivan, DW, Harrison, M, Hendler, A, Herndon, SC, Kolb, CE, Fraser, MP, Hill, AD, Lamb, BK, Miskimins, J, Sawyer, RF, Seinfeld JH. 2013. Methane emissions at natural gas production sites. *Proc Natl Acad Sci USA* **110**(44): 17768–17773. DOI: http://dx.doi.org/10.1073/pnas.1304880110.

Alvarez, RA, Zavala-Araiza, D, Lyon, DR, Allen, DT, Barkley, ZR, Brandt, AR, Davis, KJ, Herndon, SC, Jacob, DJ, Karion, A, Kort, EA, Lamb, BK, Lauvaux, T, Maasakkers, JD, Marchese, AJ, Omara, M, Pacala, SW, Peischl, J, Robinson, AL, Shepson, PB, Sweeney, C, Townsend-Small, A, Wofsy, SC, Hamburg, SP. 2018. Assessment of methane emissions from the U.S. oil and gas supply chain. *Science* **361**(6398): 186–188. DOI: http://dx.doi.org/10.1126/science.aar7204.

Anderson, K, Broderick, JF, Isak Stoddard, I. 2020. A factor of two: How the mitigation plans of 'climate progressive' nations fall far short of Paris-compliant pathways. *Clim Policy*. DOI: http://dx.doi.org/10.1080/14693062.2020.1728209.

Ayers, WB Jr. 2003. Coalbed methane in the Fruitland formation, San Juan Basin, western United States: A giant unconventional gas play, in Halbouty, MT ed., *Giant oil and gas fields of the decade 1990–1999: AAPG Memoir 78*. 159–188. Available at https://pubs.geoscienceworld.org/books/book/1287/Giant-Oil-and-Gas-Fields-of-the-Decade-1990-1999.

Baasandorj, M, Hoch, SW, Bares, R, Lin, JC, Brown, SS, Millet, DB, Martin, R, Kelly, K, Zarzana, KJ, Whiteman, CD, Dube, WP, Tonnesen, G, Jaramillo, IC, Sohl, J. 2017. Coupling between chemical and meteorological processes under persistent cold-air pool conditions: Evolution of wintertime PM2.5 pollution events and N_2O_5 observations in Utah's Salt Lake valley. *Environ Sci Technol* **51**(11): 5941–5950. DOI: http://dx.doi.org/10.1021/acs.est.6b06603.

Baker Hughes. 2015. North America Rotary Rig Count Pivot Table. Available at https://bakerhughesrigcount.gcs-web.com/. Accessed 30 June 2020.

Barnes, FC. 1951. History of development and production of oil and gas in the San Juan Basin, in Smith, CT, Silver, C eds., *San Juan Basin (New Mexico and Arizona)*. New Mexico Geological Society 2nd Annual Fall Field Conference Guidebook, 163 p. 155–160.

Bell, CS, Vaughn, TL, Zimmerle, D, Herndon, SC, Yacovitch, TI, Heath, GA, Pétron, G, Edie, R, Field, RA, Murphy, SM, Robertson, AM, Soltis, J. 2017. Comparison of methane emission estimates from multiple measurement techniques at natural gas production pads. *Elem Sci Anth* **5**: 79. DOI: http://dx.doi.org/10.1525/elementa.266.

Bianco, L, Wilczak, JM, White, AB. 2008. Convective boundary layer depth estimation from wind profilers: Statistical comparison between an automated algorithm and expert estimations. *J Atmos Ocean Tech* **25**(8): 1397–1413. DOI: http://dx.doi.org/10.1175/2008JTECHA981.1.

Bieberman, RA, Clarich, M. 1951. Mineral resources of the San Juan Basin, in Smith, CT, Silver, C eds., *San Juan Basin (New Mexico and Arizona)*. New Mexico Geological Society 2nd Annual Fall Field Conference Guidebook, 163 p., 141–146.

Brandt, AR, Heath, GA, Cooley, D. 2016. Methane leaks from natural gas systems follow extreme distributions. *Environ Sci Technol* **50**(22): 12512–12520. DOI: http://dx.doi.org/10.1021/acs.est.6b04303.

Brandt, AR, Heath, GA, Kort, EA, O'Sullivan, F, Pétron, G, Jordaan, SM, Tans, P, Wilcox, J, Gopstein, AM. 2014. Methane leaks from North American natural gas systems. *Science* **343**(6172): 733–735. DOI: http://dx.doi.org/10.1126/science.1247045.

Bruhwiler, LM, Basu, S, Bergamaschi, P, Bousquet, P, Dlugokencky, E, Houweling, S, Ishizawa, M, Kim, H-S, Locatelli, R, Maksyutov, S, Montzka, S, Pandey, S, Patra, PK, Petron, G, Saunois, M, Sweeney, C, Schwietzke, S, Tans, P, Weatherhead EC. 2017. U.S. CH_4 emissions from oil and gas production: Have recent large increases been detected? *J Geophys Res Atmos* **122**: 4070– 4083. DOI: http://dx.doi.org/10.1002/2016JD026157.

Buchwitz, M, de Beek, R, Burrows, JP, Bovensmann, H, Warneke, T, Notholt, J, Meirink, JF, Goede, APH, Bergamaschi, P, Körner, S, Heimann, M, Schulz, A. 2005. Atmospheric methane and carbon dioxide from SCIAMACHY satellite data: Initial comparison with chemistry and transport models. *Atmos Chem Phys* **5**: 941–962. DOI: http://dx.doi.org/10.5194/acp-5-941-2005.

Buchwitz, M, Reuter, M, Schneising, O, Boesch, H, Guerlet, S, Dils, B, Aben, I, Armante, R, Bergamaschi, P, Blumenstock, T, Bovensmann, H, Brunner, D, Buchmann, B, Burrows, JP, Butz, A, Chedin, A, Chevallier, F, Crevoisier, CD, Deutscher, NM, Frankenberg, C, Hase, F, Hasekamp, OP, Heymann, J, Kaminski, T, Laeng, A, Lichtenberg, G, De Maziere, M, Noel, S, Notholt, J, Orphal, J, Popp, C, Parker, R, Scholze, M, Sussmann, R, Stiller, GP, Warneke, T, Zehner, C, Bril, A, Crisp, D, Griffith, DWT, Kuze, A, O'Dell, C, Oshchepkov, S, Sherlock, V, Suto, H, Wennberg, P, Wunch, D, Yokota, T, Yoshida, Y. 2015. The Greenhouse Gas Climate Change Initiative (GHG-CCI): Comparison and quality assessment of near-surface-sensitive satellite-derived CO_2 and CH_4 global data sets. *Remote Sens Environ* **162**: 344–362.

Butler, JH, Montzka, SAM. 2018. The NOAA Annual Greenhouse Gas Index (AGGI). Published Online Spring 2018. Available at https://www.esrl.noaa.gov/gmd/aggi/aggi.html. Accessed 30 June 2020.

COGCC/LTE. 2018. *San Juan Basin 3 M Project—Fruitland outcrop monitoring reports*. Available at https://cogcc.state.co.us/library.html#/areareports. Accessed 30 June 2020.

Colorado Oil and Gas Conservation Commission Data (COGCC). 2018. *Production by county*. Available at https://cogcc.state.co.us/data.html#/cogis. Accessed 30 June 2020.

Conley, SA, Faloona, I, Mehrotra, S, Suard, M, Lenschow, DH, Sweeney, C, Herndon, S, Schwietzke, S, Pétron, G, Pifer, J, Kort, EA, Schnell, R. 2017. Application of Gauss's theorem to quantify localized surface emissions from

airborne measurements of wind and trace gases. *Atmos Meas Tech* **10**: 3345–3358. DOI: http://dx.doi.org/10.5194/amt-10-3345-2017.

Conley, SA, Faloona, IC, Lenschow, DH, Karion, A, Sweeney, C. 2014. A low-cost system for measuring horizontal winds from single-engine aircraft. *J Atmos Oceanic Technol* **31**: 1312–1320. DOI: http://dx.doi.org/10.1175/JTECH-D-13-00143.1.

Cusworth, DH, Duren, RM, Thorpe, AK, Tseng, E, Thompson, D, Guha, A, Newman, S, Foster, KT, Miller, CE. 2020. Using remote sensing to detect, validate, and quantify methane emissions from California solid waste operations. *Environ Res Lett* **15**: 054012. DOI: http://dx.doi.org/10.1088/1748-9326/ab7b99.

Cusworth, DH, Jacob, DJ, Sheng, JX, Benmergui, J, Turner, AJ, Brandman, J, White, L, Randles, CA. 2018. Detecting high-emitting methane sources in oil/gas fields using satellite observations. *Atmos Chem Phys* **18**(23): 16885–16896. DOI: http://dx.doi.org/10.5194/acp-18-16885-2018.

de Gouw, JA, Veefkind, JP, Roosenbrand, E, Dix, B, Lin, JC, Landgraf, J, Levelt, PF. 2020. Daily satellite observations of methane from oil and gas production regions in the United States. *Nat Sci Rep* **10**: 1379. DOI: http://dx.doi.org/10.1038/s41598-020-57678-4.

de Gouw, JA, Te Lintel Hekkert, S, Mellqvist, J, Warneke, C, Atlas, EL, Fehsenfeld, FC, Fried, A, Frost, GJ, Harren, FJM, Holloway, JS, Lefer, B, Lueb, R, Meagher, JF, Parrish, DD, Patel, M, Pope, L, Richter, D, Rivera, C, Ryerson, TB, Samuelsson, J, Walega, J, Washenfelder, RA, Weibring, P, Zhu, X. 2009. Airborne measurements of ethene from industrial sources using laser photo-acoustic spectroscopy. *Environ Sci Technol* **43**(7): 2437–2442. DOI: http://dx.doi.org/10.1021/es802701a.

Dlugokencky, EJ. 2019. NOAA/ESRL. Available at www.esrl.noaa.gov/gmd/ccgg/trends_ch4/. Accessed 30 June 2020.

Dlugokencky, EJ, Bruhwiler, L, White, JWC, Emmons, L, Novelli, PC, Montzka, SA, Masarie, KA, Lang, PM, Crotwell, AM, Miller, JB, Gatti, LV. 2009. Observational constraints on recent increases in the atmospheric CH_4 burden. *Geophys Res Lett* **36**: L18803. DOI: http://dx.doi.org/10.1029/2009GL039780.

Dlugokencky, EJ, Myers, RC, Lang, PM, Masarie, KA, Crotwell, AM, Thoning, KW, Hall, BD, Elkins, JW, Steele, LP. 2005. Conversion of NOAA atmospheric dry air CH_4 mole fractions to a gravimetrically prepared standard scale. *J Geophys Res* **110**: D18306. DOI: http://dx.doi.org/10.1029/2005JD006035.

Dlugokencky, EJ, Nisbet EG, Fisher, R, Lowry, D. 2011. Global atmospheric methane: Budget, changes and dangers. *Philos Trans R Soc A* **369**(1943): 2058–2072. DOI: http://dx.doi.org/10.1098/rsta.2010.0341.

Dlugokencky, EJ, Steele, LP, Lang, PM, Masarie, KA. 1994. The growth rate and distribution of atmospheric methane. *J Geophys Res* **99**: 17021–17043. DOI: http://dx.doi.org/10.1029/94JD01245.

EPA Greenhouse Gas Inventory. 2020. Inventory of U.S. Greenhouse Gas Emissions and Sinks: 1990–2018. Available at https://www.epa.gov/ghgemissions/inventory-us-greenhouse-gas-emissions-and-sinks. Accessed 17 August 2020.

EPA Greenhouse Gas Reporting Program Data. 2018. Available at https://www.epa.gov/ghgreporting. Accessed 30 June 2020.

Etheridge, DM, Steele, LP, Francey, RJ, Langenfelds, RI. 2002. Historical CH_4 records since about 1000 A.D. from ice core data, in *Trends: A compendium of data on global change*. Oak Ridge, TN: Carbon Dioxide Information Analysis Center, Oak Ridge National Laboratory, U.S. Department of Energy.

Fassett, JE, Boyce, BC. 2005. Fractured-sandstone gas reservoirs, San Juan Basin, New Mexico and Colorado: Stratigraphic traps, not basin centered gas deposits—With an overview of Fruitland formation coal-bed methane, in Bishop, MG, Cumella, SP, Robinson, JW, Silverman, MR eds., *Gas in low permeability reservoirs of the Rocky Mountain Region*. Denver, CO: Rocky Mountain Association of Geologists: 109–185.

Fassett, JE, Hinds, JS. 1971. Geology and fuel resources of the Fruitland formation and Kirtland Shale of the San Juan Basin, New Mexico and Colorado. Geological Survey Professional Paper 676, 76 p.

Fast, JD, de Foy, B, Acevedo Rosas, F, Caetano, E, Carmichael, G, Emmons, L, McKenna, D, Mena, M, Skamarock, W, Tie, X, Coulter, RL, Barnard, JC, Wiedinmyer, C, Madronich, S. 2007. A meteorological overview of the MILAGRO field campaigns. *Atmos Chem Phys* **7**: 2233–2257. DOI: http://dx.doi.org/10.5194/acp-7–2233-2007.

Franco, B, Mahieu, E, Emmons, LK, Tzompa-Sosa, ZA, Fischer, EV, Sudo, K, Bovy, B, Conway, S, Griffin, D, Hannigan, JW. 2016. Evaluating ethane and methane emissions associated with the development of oil and natural gas extraction in North America. *Environ Res Lett* **11**(4): 11. DOI: http://dx.doi.org/10.1088/1748-9326/11/4/044010.

Frankenberg, C, Aben, I, Bergamaschi, P, Dlugokencky, EJ, van Hees, R, Houweling, S, van der Meer, P, Snel, R, Tol, P. 2011. Global column-averaged methane mixing ratios from 2003 to 2009 as derived from SCIAMACHY: Trends and variability. *J Geophys Res* **116**: D04302. DOI: http://dx.doi.org/10.1029/2010JD014849.

Frankenberg, C, Meirink, JF, Bergamaschi, P, Goede, APH, Heimann, M, Körner, S, Platt, U, van Weele, M, Wagner, T. 2006. Satellite chartography of atmospheric methane from SCIAMACHY on board ENVISAT: Analysis of the years 2003 and 2004. *J Geophys Res* **111**: D07303. DOI: http://dx.doi.org/10.1029/2005JD006235.

Frankenberg, C, Thorpe, AK, Thompson, DR, Hulley, G, Kort, EA, Vance, N, Borchardt, J, Krings, T, Gerilowski, K, Sweeney, C, Conley, S, Bue, BD,

Aubrey, AD, Hook, A, Green, RO. 2016. Airborne methane remote measurements reveal heavy-tail flux distribution in Four Corners region. *Proc Natl Acad Sci USA* **113**(35): 9734–9739. DOI: http://dx.doi.org/10.1073/pnas.1605617113.

Geibel, MC, Messerschmidt, J, Gerbig, C, Blumenstock, T, Chen, H, Hase, F, Kolle, O, Lavrič, JV, Notholt, J, Palm, M, Rettinger, M, Schmidt, M, Sussmann, R, Warneke, T, Feist, DG. 2012. Calibration of column-averaged CH_4 over European TCCON FTS sites with airborne in-situ measurements. *Atmos Chem Phys* **12**: 8763–8775. DOI: http://dx.doi.org/10.5194/acp-12-8763-2012.

Gerber, PJ, Steinfeld, H, Henderson, B, Mottet, A, Opio, C, Dijkman, J, Falcucci, A, Tempio, G. 2013. *Tackling climate change through livestock—A global assessment of emissions and mitigation opportunities*. Rome: Food and Agriculture Organization of the United Nations.

GML CH_4 Scale. 2015. *Methane WMO Scale: Scale update: WMO X2004A*. Available at https://www.esrl.noaa.gov/gmd/ccl/ch4_scale.html. Accessed 17 August 2020.

Haldar, SK. 2018. Elements of mining, in *Mineral exploration*. Second edition. Principles and Applications: 229–258. DOI: http://dx.doi.org/10.1016/B978-0-12-814022-2.00012-5.

Hall, BD, Crotwell, AM, Miller, BR, Schibig, M, Elkins, JW. 2019. Gravimetrically prepared carbon dioxide standards in support of atmospheric research. *Atmos Meas Tech* **12**: 517–524. DOI: http://dx.doi.org/10.5194/amt-12-517-2019.

Hausmann, P, Sussmann, R, Smale, D. 2016. Contribution of oil and natural gas production to renewed increase in atmospheric methane (2007–2014): Top–down estimate from ethane and methane column observations. *Atmos Chem Phys* **16**: 3227–3244. DOI: http://dx.doi.org/10.5194/acp-16-3227-2016.

He, J, Naik, V, Horowitz, LW, Dlugokencky, E, Thoning, K. 2020. Investigation of the global methane budget over 1980-2017 using GFDL-AM4.1. *Atmos Chem Phys* **20**: 805–827. DOI: http://dx.doi.org/10.5194/acp-2019-529.

Helmig, D, Rossabi, S, Hueber, J, Tans, P, Montzka, SA, Masarie, K, Thoning, K, Plass-Duelmer, C, Claude, A, Carpenter, LJ, Lewis, AC, Punjabi, S, Reimann, S, Vollmer, MK, Steinbrecher, R, Hannigan, JW, Emmons, LK, Mahieu, E, Franco, B, Smale, D, Pozzer, A. 2016. Reversal of global atmospheric ethane and propane trends largely due to US oil and natural gas production. *Nat Geosci* **9**(7): 490–495. DOI: http://dx.doi.org/10.1038/ngeo2721.

Helmig, D, Thompson, CR, Evans, J, Boylan, P, Hueber, J, Park, JH, 2014. Highly elevated atmospheric levels of volatile organic compounds in the Uintah Basin, Utah. *Environ Sci Technol* **48**(9): 4707–4715. DOI: http://dx.doi.org/10.1021/es405046r.

Hopkins, FM, Kort, EA, Bush, SE, Ehleringer, JR, Lai, CT, Blake, DR, Randerson, JT. 2016. Spatial patterns and source attribution of urban methane in the Los Angeles Basin. *J Geophys Res Atmos* **121**: 2490–2507. DOI: http://dx.doi.org/10.1002/2015JD024429.

Horton, BP, Kopp, RE, Garner, AJ, Hay, CC, Khan, NS, Roy, K, Shaw, TA. 2018. Mapping sea-level change in time, space, and probability. *Annu Rev Environ Resourc* **43**: 481–521.

Hübler, G, Alvarez, R, Daum, P, Dennis, R, Gillani, N, Kleinman, L, Luke, W, Meagher, J, Rider, D, Trainer, M, Valente, R. 1998. An overview of the airborne activities during the Southern Oxidants Study (SOS) 1995 Nashville/Middle Tennessee Ozone Study. *J Geophys Res Atmos* **103**: 22245–22259. DOI: http://dx.doi.org/10.1029/98JD01638.

Huffman, AC Jr, Condon, SM. 1993. Stratigraphy, structure, and paleogeography of Pennsylvanian and Permian rocks, San Juan Basin and adjacent areas, Utah, Colorado, Arizona, and New Mexico. USGS Bulletin 1808-O, pp. 1–44.

ICF International. 2016. Summary of methane emission reduction opportunities across North American oil and natural gas industries. Report prepared for the Environmental Defense Fund, 9 p. Available at https://www.edf.org/sites/default/files/north-american-executive-summary_english.pdf. Accessed 30 June 2020.

IPCC. 2018. Global warming of 1.5°C. An IPCC special report on the impacts of global warming of 1.5°C above pre-industrial levels and related global greenhouse gas emission pathways, in the context of strengthening the global response to the threat of climate change, sustainable development, and efforts to eradicate poverty, in Masson-Delmotte, V, Zhai, P, Pörtner, HO, Roberts, D, Skea, J, Shukla, PR, Pirani, A, Moufouma-Okia, W, Péan, C, Pidcock, R, Connors, S, Matthews, JBR, Chen, Y, Zhou, X, Gomis, MI, Lonnoy, E, Maycock, T, Tignor, M, Waterfield, T eds. Available at https://www.ipcc.ch/sr15/. Accessed 30 June 2020.

Jacob, DJ, Turner, AJ, Maasakkers, JD, Sheng, J, Sun, K, Liu, X, Chance, K, Aben, I, McKeever, J, Frankenberg, C. 2016. Satellite observations of atmospheric methane and their value for quantifying methane emissions. *Atmos Chem Phys* **16**: 14371–14396. DOI: http://dx.doi.org/10.5194/acp-16-14371-2016.

Jeong, S, Newman, S, Zhang, J, Andrews, AE, Bianco, L, Bagley, J, Cui, X, Graven, H, Kim, J, Salameh, P, LaFranchi, BW, Priest, C, Campos-Pineda, M, Novakovskaia, E, Sloop, CD, Michelsen, HA, Bambha, RP, Weiss, RF, Keeling, R, Fischer, ML. 2016. Estimating methane emissions in California's urban and rural regions using multitower observations. *J Geophys Res Atmos* **121**: 13031–13049. DOI: http://dx.doi.org/10.1002/2016JD025404.

Johnson, KA, Johnson, DE. 1995. Methane emissions from cattle. *J Anim Sci* **73**(8): 2483–2492.

Karion, A, Sweeney, C, Kort, EA, Shepson, PB, Brewer, A, Cambaliza, M, Conley, SA, Davis, K, Deng, A, Hardesty, M, Herndon, SC, Lauvaux, T, Lavoie, T, Lyon, D, Newberger, T, Pétron, G, Rella, C, Smith, M, Wolter, S, Yacovitch, TI, Tans, P. 2015. Aircraft-based estimate of total methane emissions from the Barnett Shale Region. *Environ Sci Technol* **49**: 8124–8131. DOI: http://dx.doi.org/10.1021/acs.est.5b00217.

Karion, A, Sweeney, C, Pétron, G, Frost, G, Hardesty, RM, Kofler, J, Miller, BR, Newberger, T, Wolter, S, Banta, R, Brewer, A, Dlugokencky, E, Lang, P, Montzka, SA, Schnell, R, Tans, P, Trainer, M, Zamora, R, Conley, S. 2013. Methane emissions estimate from airborne measurements over a western United States natural gas field. *Geophys Res Lett* **40**: 4393–4397. DOI: http://dx.doi.org/10.1002/grl.50811.

Katzenstein, AS, Doezema, LA, Simpson, IJ, Balke, DR, Rowland, FS. 2003. Extensive regional atmospheric hydrocarbon pollution in the southwestern United States. *Proc Natl Acad Sci USA* **100**(21): 11975–11979. DOI: http://dx.doi.org/10.1073/pnas.1635258100.

Kort, EA, Frankenberg, C, Costigan, KR, Lindenmaier, R, Dubey, MK, Wunch, D. 2014. Four corners: The largest US methane anomaly viewed from space. *Geophys Res Lett* **41**: 6898–6903. DOI: http://dx.doi.org/10.1002/2014GL061503.

Lawrence, JP, Anand, JS, Vande Hey, JD, White, J, Leigh, RR, Monks, PS, Leigh, RJ. 2015. High-resolution measurements from the airborne Atmospheric Nitrogen Dioxide Imager (ANDI). *Atmos Meas Tech* **8**: 4735–4754. DOI: http://dx.doi.org/10.5194/amt-8-4735-2015.

Littman, FE, Magill, PL. 1953. Some unique aspects of air pollution in Los Angeles. *Air Repair* **3**(1): 29–34. DOI: http://dx.doi.org/10.1080/00966665.1953.10467586.

Loew, A, Bell, W, Brocca, L, Bulgin, CE, Burdanowitz, J, Calbet, X, Donner, RV, Ghent, D, Gruber, A, Kaminski, T, Kinzel, J, Klepp, C, Lambert, J-C, Schaepman-Strub, G, Schröder, M, Verhoelst, T. 2017. Validation practices for satellite-based Earth observation data across communities. *Rev Geophys* **55**: 779–817. DOI: http://dx.doi.org/10.1002/2017RG000562.

Loulergue, L, Schilt, A, Spahni, R, Masson-Delmotte, V, Blunier, T, Lemieux, B, Barnola, JM, Raynaud, D, Stocker, TF, Chappellaz, J. 2008. Orbital and millennial-scale features of atmospheric CH_4 over the past 800,000 years. *Nature* **453**: 383–386. DOI: http://dx.doi.org/10.1038/nature06950.

LTE. 2015. 2015 Fruitland outcrop monitoring report. La Plata County, CO. Available at https://cogcc.state.co.us/documents/library/AreaReports/SanJuanBasin/3m_project/2015%20FRUITLAND%20OUTCROP%20MONITORING%20REPORT_La_Plata.pdf. Accessed 30 June 2020.

LTE. 2017. Fruitland Formation outcrop methane flux measurements 2007–2017 and converting fugitive methane gas emissions into a viable resource, Ager et al. presentation at the 2017 Four Corners Air Quality Group meeting in Durango, 9-12-2017. Available at https://www.env.nm.gov/air-quality/fcaqg/, under Meetings tab. Accessed 30 June 2020.

Lyon, DR, Alvarez, RA, Zavala-Araiza, D, Brandt, AR, Jackson, RB, Hamburg, SP. 2016. Aerial surveys of elevated hydrocarbon emissions from oil and gas production sites. *Environ Sci Technol* **50**: 4877–4886. DOI: http://dx.doi.org/10.1021/acs.est.6b00705.

Lyon, DR, Zavala-Araiza, D, Alvarez, RA, Harriss, R, Palacios, V, Lan, X, Talbot, R, Lavoie, T, Shepson, P, Yacovitch, TI, Herndon, SC, Marchese, AJ, Zimmerle, D, Robinson, AL, Hamburg, SP. 2015. Constructing a spatially resolved methane emission inventory for the Barnett Shale region. *Environ Sci Technol* **49**(13): 8147–8157. DOI: http://dx.doi.org/10.1021/es506359c.

Maasakkers, JD, Jacob, DJ, Sulprizio, MP, Turner, AJ, Weitz, M, Wirth, T, Hight, C, DeFigueiredo, M, Desai, M, Schmeltz, R, Hockstad, L, Bloom, AA, Bowman, KW, Jeong, S, Fischer, ML. 2016. Gridded national inventory of U.S. methane emissions. *Environ Sci Technol* **50**(23): 13123–13133. DOI: http://dx.doi.org/10.1021/acs.est.6b02878.

Marchese, AJ, Vaughn, TL, Zimmerle, DJ, Martinez, DM, Williams, LL, Robinson, AL, Mitchell, AL, Subramanian, R, Tkacik, DS, Roscioli, JR, Herndon, SC. 2015. Methane emissions from United States natural gas gathering and processing. *Environ Sci Technol* **49**(17): 10718–10727. DOI: http://dx.doi.org/10.1021/acs.est.5b02275.

Mielke-Maday, I, Schwietzke, S, Yacovitch, T, Miller, B, Conley, S, Kofler, J, Handley, P, Thorley, E, Herndon, SC, Hall, B, Dlugokencky, E, Lang, P, Wolter, S, Moglia, E, Crotwell, M, Crotwell, A, Rhodes, M, Kitzis, D, Vaughn, T, Bell, C, Zimmerle, D, Schnell, R, Pétron, G. 2019. Methane source attribution in a U.S. dry gas basin using spatial patterns of ground and airborne ethane and methane measurements. *Elem Sci Anth* **7**(1): 13. DOI: http://dx.doi.org/10.1525/elementa.351.

Mielke-Maday, I. 2019. Source attribution of hydrocarbons with potential for impacts on climate and human health from oil and natural gas production [PhD thesis]. Boulder, CO: University of Colorado, 230 p. Available at https://pqdtopen.proquest.com/doc/2335180942.html?FMT=ABS. Accessed 30 June 2020.

Miller, SM, Wofsy, SC, Michalak, AM, Kort, EA, Andrews, AE, Biraud, SC, Dlugokencky, EJ, Eluszkiewicz, J, Fischer, ML, Janssens-Maenhout, G, Miller, BR, Miller, JB, Montzka, SA, Nehrkorn, T, Sweeney, C. 2013. Anthropogenic emissions of methane in the United States. *Proc Natl Acad Sci USA* **110**(50): 20018–20022. DOI: http://dx.doi.org/10.1073/pnas.1314392110.

Montzka, S, Dlugokencky, E, Butler, J. 2011. Non-CO_2 greenhouse gases and climate change. *Nature* **476**: 43–50. DOI: http://dx.doi.org/10.1038/nature10322.

Murray, DK. 1996. Coalbed methane in the USA: Analogues for worldwide development, in Gayer, R, Harris, I. eds., *Coalbed methane and coal geology*. London: Geological Society, Special Publication No 109, pp. 1–12.

New Mexico Oil Conservation Division Statistics. 2018. County production and injection by month. Available at http://www.emnrd.state.nm.us/OCD/statistics.html. Accessed 30 June 2020.

Nickelson, HB. 1988. One hundred years of coal mining in the San Juan Basin, New Mexico, Bulletin 111, NM Bureau of Mines & Mineral Resources. Available at https://geoinfo.nmt.edu/publications/monographs/bulletins/downloads/111/B111.pdf. Accessed 30 June 2020.

Nisbet, EG, Fisher, RE, Lowry, D, France, JL, Allen, G, Bakkaloglu, S, Broderick, TJ, Cain, M, Coleman, M, Fernandez, J, Forster, G, Griffiths, PT, Iverach, CP, Kelly, BFJ, Manning, MR, Nisbet-Jones, PBR, Pyle, JA, Townsend-Small, A, al-Shalaan, A, Warwick, N, Zazzeri, G. 2020. Methane mitigation: Methods to reduce emissions, on the path to the Paris agreement. *Rev Geophys* **58**. DOI: http://dx.doi.org/10.1029/2019RG000675.

Nisbet, EG, Manning, MR, Dlugokencky, EJ, Fisher, RE, Lowry, D, Michel, SE, Myhre, CL, Platt, SM, Allen, G, Bousquet, P, Brownlow, R, Cain, M, France, JL, Hermansen, O, Hossaini, R, Jones, AE, Levin, I, Manning, AC, Myhre, G, Pyle, JA, Vaughn, BH, Warwick, NJ, White, JWC. 2019. Very strong atmospheric methane growth in the 4 years 2014–2017: Implications for the Paris Agreement. *Global Biogeochem Cycles* **33**: 318–342. DOI: http://dx.doi.org/10.1029/2018GB006009.

Oltmans, S, Schnell, R, Johnson, B, Pétron, G, Mefford, T, Neely, R III. 2014. Anatomy of wintertime ozone associated with oil and natural gas extraction activity in Wyoming and Utah. *Elem Sci Anth*. DOI: http://dx.doi.org/10.12952/journal.elementa.000024.

Pandey, S, Gautam, R, Houweling, S, van der Gon, HD, Sadavarte, P, Borsdorff, T, Hasekamp, O, Landgraf, J, Tol, P, van Kempen, T, Hoogeveen, R, van Hees, R, Hamburg, SP, Maasakkers, JD, Aben, I. 2019. Satellite observations reveal extreme methane leakage from a natural gas well blowout. *Proc Natl Acad Sci USA* **116**: 26376–26381. DOI: http://dx.doi.org/10.1073/pnas.1908712116.

Parikh, R, Grant, J, Bar-Ilan, A. 2017a. Development of baseline 2014 emissions from oil and gas activity in Greater San Juan Basin and Permian Basin, Final Report. Available at https://www.wrapair2.org/pdf/2014_SanJuan_Permian_Baseyear_EI_Final_Report_10Nov2017.pdf. Accessed 31 August 2020.

Parikh, R, Grant, J, Bar-Ilan, A. 2017b. Greater San Juan Basin 2014 EI spreadsheet. Available at https://www.wrapair2.org/pdf/2014_San_Juan_Basin_O&G_EI_Summary_082917.xlsx. Accessed 31 August 2020.

Peischl, J, Eilerman, SJ, Neuman, JA, Aikin, KC, de Gouw, J, Gilman, JB, Herndon, SC, Nadkarni, R, Trainer, M, Warneke, C, Ryerson, TB. 2018. Quantifying methane and ethane emissions to the atmosphere from central and western U.S. oil and natural gas production regions. *J Geophys Res Atmos* **123**. DOI: http://dx.doi.org/10.1029/2018JD028622.

Peischl, J, Karion, A, Sweeney, C, Kort, EA, Smith, ML, Brandt, AR, Yeskoo, T, Aikin, KC, Conley, SA, Gvakharia, A, Trainer, M, Wolter, S, Ryerson, TB. 2016. Quantifying atmospheric methane emissions from oil and natural gas production in the Bakken shale region of North Dakota. *J Geophys Res Atmos* **121**: 6101–6111. DOI: http://dx.doi.org/10.1002/2015JD024631.

Peischl, J, Ryerson, TB, Aikin, KC, de Gouw, JA, Gilman, JB, Holloway, JS, Lerner, BM, Nadkarni, R, Neuman, JA, Nowak, JB, Trainer, M, Warneke, C, Parrish, DD. 2015. Quantifying methane emissions from the Haynesville, Fayetteville, and Marcellus shale play regions. *J Geophys Res Atmos* **120**: 2119–2139. DOI: http://dx.doi.org/10.1002/2014JD022697.

Pétron, G, Karion, A, Sweeney, C, Miller, BR, Montzka, SA, Frost, GJ, Trainer, M, Tans, P, Andrews, A, Kofler, J, Helmig, D, Guenther, D, Dlugokencky, E, Lang, P, Newberger, T, Wolter, S, Hall, B, Novelli, P, Brewer, A, Conley, S, Hardesty, M, Banta, R, White, A, Noone, D, Wolfe, D, Schnell, R. 2014. A new look at methane and nonmethane hydrocarbon emissions from oil and natural gas operations in the Colorado Denver-Julesburg Basin. *J Geophys Res Atmos* **119**: 6836–6852. DOI: http://dx.doi.org/10.1002/2013JD021272.

Reddy, PJ, Pfister, GG. 2016. Meteorological factors contributing to the interannual variability of midsummer surface ozone in Colorado, Utah, and other western U.S. states. *J Geophys Res Atmos* **121**: 2434–2456. DOI: http://dx.doi.org/10.1002/2015JD023840.

Rella, CW, Tsai, TR, Botkin, CG, Crosson, ER, Steele, D. 2015. Measuring emissions from oil and natural gas well pads using the Mobile Flux Plane technique. *Environ Sci Technol* **49**(7): 4742–4748. DOI: http://dx.doi.org/10.1021/acs.est.5b00099.

Rice, DD. 1993. Composition and origins of coalbed gas. *AAPG Studies in Geology* **38**: 159–184.

Ridgley, JL, Condon, SM, Hatch, JR. 2013. Geology and oil and gas assessment of the Fruitland total petroleum system, San Juan Basin, New Mexico and Colorado, in Total Petroleum Systems and Geologic Assessment of Undiscovered Oil and Gas Resources in the San Juan Basin Province, Exclusive of Paleozoic Rocks, New Mexico and Colorado, USGS, Chap. 6, 100 pp. Available at https://pubs.usgs.gov/dds/dds-069/dds-069-f/

REPORTS/Chapter6_508.pdf. Accessed 30 June 2020.

Saunois, M, Bousquet, P, Poulter, B, Peregon, A, Ciais, P, Canadell, JG, Dlugokencky, EJ, Etiope, G, Bastviken, D, Houweling, S, Janssens-Maenhout, G, Tubiello, FN, Castaldi, S, Jackson, RB, Alexe, M, Arora, VK, Beerling, DJ, Bergamaschi, P, Blake, DR, Brailsford, G, Brovkin, V, Bruhwiler, L, Crevoisier, C, Crill, P, Covey, K, Curry, C, Frankenberg, C, Gedney, N, Höglund-Isaksson, L, Ishizawa, M, Ito, A, Joos, F, Kim, H-S, Kleinen, T, Krummel, P, Lamarque, J-F, Langenfelds, R, Locatelli, R, Machida, T, Maksyutov, S, McDonald, KC, Marshall, J, Melton, JR, Morino, I, Naik, V, O'Doherty, S, Parmentier, F-JW, Patra, PK, Peng, C, Peng, S, Peters, GP, Pison, I, Prigent, C, Prinn, R, Ramonet, M, Riley, WJ, Saito, M, Santini, M, Schroeder, R, Simpson, IJ, Spahni, R, Steele, P, Takizawa, A, Thornton, BF, Tian, H, Tohjima, Y, Viovy, N, Voulgarakis, A, van Weele, M, van der Werf, GR, Weiss, R, Wiedinmyer, C, Wilton, DJ, Wiltshire, A, Worthy, D, Wunch, D, Xu, X, Yoshida, Y, Zhang, B, Zhang, Z, Zhu, Q. 2016. The global methane budget 2000–2012, *Earth Syst Sci Data* **8**: 697–751. DOI: http://dx.doi.org/10.5194/essd-8-697-2016.

Schnell, RC, Oltmans, SJ, Neely, RR, Endres, MS, Molenar, JV, White, AB. 2009. Rapid photochemical production of ozone at high concentrations in a rural site during winter. *Nat Geosci* **2**(2): 120–122. DOI: http://dx.doi.org/10.1038/ngeo415.

Schwietzke, S, Harrison, M, Lauderdale, T, Branson, K, Conley, S, George, FC, Jordan, D, Jersey, GR, Zhang, C, Mairs, HL, Pétron, G, Schnell, RC. 2018. Aerially guided leak detection and repair: A pilot field study for evaluating the potential of methane emission detection and cost-effectiveness. *J Air Waste Manag Assoc* **69**(1): 71–88. DOI: http://dx.doi.org/10.1080/10962247.2018.1515123.

Schwietzke, S, Pétron, G, Conley, S, Pickering, C, Mielke-Maday, I, Dlugokencky, EJ, Tans, PP, Vaughn, T, Bell, C, Zimmerle, D, Wolter, S, King, CW, White, AB, Coleman, T, Bianco, L, Schnell, RC. 2017. Improved mechanistic understanding of natural gas methane emissions from spatially resolved aircraft measurements. *Env Sc Tech* **51**(12): 7286–7294. DOI: http://dx.doi.org/10.1021/acs.est.7b01810.

Schwietzke, S, Sherwood, OA, Bruhwiler, LMP, Miller, JB, Etiope, G, Dlugokencky, EJ, Michel, SE, Arling, VA, Vaughn, BH, White, JWC, Tans, PP. 2016. Upward revision of global fossil fuel methane emissions based on isotope database. *Nature* **538**: 88–91. DOI: http://dx.doi.org/10.1038/nature19797.

Sherwood, OA, Schwietzke, S, Arling, VA, Etiope, G. 2017. Global inventory of gas geochemistry data from fossil fuel, microbial and burning sources, version 2017. *Earth Syst Sci Data* **9**: 639–656. DOI: http://dx.doi.org/10.5194/essd-9-639-2017.

Sherwood, OA, Travers, PD, Dolan, MP. 2013. Chapter 15—Compound-specific stable isotope analysis of natural and produced hydrocarbon gases surrounding oil and gas operations. *Compr Anal Chem* **61**: 347–372. DOI: http://dx.doi.org/10.1016/B978-0-444-62623-3.00015-0.

Shim, C, Han, J, Henze, DK, Yoon, T. 2018. Identifying local anthropogenic CO_2 emissions with satellite retrievals: A case study in South Korea. *Int J Remote Sensing* **40**(3): 1011–1029. DOI: http://dx.doi.org/10.1080/01431161.2018.1523585.

Smith, ML, Gvakharia, A, Kort, EA, Sweeney, C, Conley, SA, Faloona, I, Newberger, T, Schnell, R, Schwietzke, S, Wolter, S. 2017. Airborne quantification of methane emissions over the four corners region. *Environ Sci Technol* **51**(10): 5832–5837. DOI: http://dx.doi.org/10.1021/acs.est.6b06107.

Smith, ML, Kort, EA, Karion, A, Sweeney, C, Herndon, SC, Yacovitch, TI. 2015. Airborne ethane observations in the Barnett Shale: quantification of ethane flux and attribution of methane emissions. *Environ Sci Technol* **49**(13): 8158–8166. DOI: http://dx.doi.org/10.1021/acs.est.5b00219s.

Stephens, S, Madronich, S, Wu, F, Olson, J, Ramos, R, Retama, A, Muñoz, R. 2008. Weekly patterns of México City's surface concentrations of CO, NOx, PM10, and O_3 during 1986–2007. *Atmos Chem Phys* **8**: 5313–5325.

Subramanian, S, Williams, LL, Vaughn, TL, Zimmerle, D, Roscioli, JR, Herndon, SC, Yacovitch, TI, Floerchinger, C, Tkacik, DS, Mitchell, AL, Sullivan, MR, Dallmann, TR, Robinson, AL. 2015. Methane emissions from natural gas compressor stations in the transmission and storage sector: Measurements and comparisons with the EPA Greenhouse Gas Reporting Program protocol. *Environ Sci Technol* **49**(5): 3252–3261. DOI: http://dx.doi.org/10.1021/es5060258.

Thompson, DR, Thorpe, AK, Frankenberg, C, Green, RO, Duren, R, Guanter, L, Hollstein, A, Middleton, E, Ong, L, Ungar, S. 2016. Space-based remote imaging spectroscopy of the Aliso Canyon CH_4 superemitter. *Geophys Res Lett* **43**: 6571–6578. DOI: http://dx.doi.org/10.1002/2016GL069079.

Thorpe, AK, Frankenberg, C, Thompson, DR, Duren, RM, Aubrey, AD, Bue, BD, Green, RO, Gerilowski, K, Krings, T, Borchardt, J, Kort, EA, Sweeney, C, Conley, S, Roberts, DA, Dennison, PE. 2017. Airborne DOAS retrievals of methane, carbon dioxide, and water vapor concentrations at high spatial resolution: Application to AVIRIS-NG. *Atmos Meas Tech* **10**: 3833–3850. DOI: http://dx.doi.org/10.5194/amt-10–3833-2017.

Tian, H, Lu, C, Ciais, P, Michalak, AM, Canadell, JG, Saikawa, E, Huntzinger, DN, Gurney, KR, Sitch, S, Zhang, B, Yang, J, Bousquet, P, Bruhwiler, L, Chen, G, Dlugokencky, E, Friedlingstein, P, Melillo, J, Pan, S, Poulter, B, Prinn, R, Saunois, M, Schwalm, CR, Wofsy, SC. 2016. The terrestrial biosphere as a net source of greenhouse gases to the

atmosphere. *Nature* **531**: 225–228. DOI: http://dx.doi.org/10.1038/nature16946.

Turner, AJ, Jacob, DJ, Benmergui, J, Wofsy, SC, Maasakkers, JD, Butz, A, Hasekamp, O, Biraud, SC. 2016. A large increase in U.S. methane emissions over the past decade inferred from satellite data and surface observations. *Geophys Res Lett* **43**: 2218–2224. DOI: http://dx.doi.org/10.1002/2016GL067987.

U.S. Department of Agriculture. 2014. 2012 Census Full Report. Available at https://www.agcensus.usda.gov/Publications/2012/. Accessed 30 June 2020.

U.S. Energy Information Agency. 2018a. *Production statistics*. Available at https://www.eia.gov/. Accessed 30 June 2020.

U.S. Energy Information Agency. 2018b. *Coalbed methane production*. Available at https://www.eia.gov/dnav/ng/ng_prod_coalbed_s1_a.htm. Accessed 30 June 2020.

USGCRP. 2018. Impacts, risks, and adaptation in the United States: Fourth National Climate Assessment, Volume II, in Reidmiller, DR, Avery, CW, Easterling, DR, Kunkel, KE, Lewis, KLM, Maycock, TK, Stewart, BC eds. Washington, DC: U.S. Global Change Research Program: 1515. DOI: http://dx.doi.org/10.7930/NCA4.2018.

USGS. 2014. USGS energy geochemistry database. Available at https://openei.org/datasets/dataset/usgs-energy-geochemistry-database. Accessed 31 August 2020.

Vanderwende, BJ, Lundquist, JK, Rhodes, ME, Takle, ES, Irvin, S. 2015. Observing and simulating the summertime low-level jet in central Iowa. *Monthly Weather Review*. DOI: http://dx.doi.org/10.1175/MWR-D-14-00325.1.

Varon, DJ, Jacob, DJ, McKeever, J, Jervis, D, Durak, BOA, Xia, Y, Huang, Y. 2018. Quantifying methane point sources from fine-scale satellite observations of atmospheric methane plumes. *Atmos Meas Tech* **11**: 5673–5686. DOI: http://dx.doi.org/10.5194/amt-11-5673-2018.

Varon, DJ, McKeever, J, Jervis, D, Maasakkers, JD, Pandey, S, Houweling, S, Aben, I, Scarpelli, T, Jacob, DJ. 2019. Satellite discovery of anomalously large methane point sources from oil/gas production. *Geophys Res Lett* **46**: 13507–13516. DOI: http://dx.doi.org/10.1029/2019GL083798.

Vaughn, TL, Bell, CS, Pickering, CK, Schwietzke, S, Heath, GA, Pétron, G, Zimmerle, DJ, Schnell, RC, Nummedal, D. 2018. Temporal variability largely explains top-down/bottom-up difference in methane emission estimates from a natural gas production region. *Proc Natl Acad Sci USA* **115**(46): 11712–11717. DOI: http://dx.doi.org/10.1073/pnas.1805687115.

Wennberg, PO, Mui, W, Wunch, D, Kort, EA, Blake, DR, Atlas, EL, Santoni, GW, Wofsy, SC, Diskin, GS, Jeong, S, Fischer, ML. 2012. On the sources of methane to the Los Angeles atmosphere. *Environ Sci Technol* **46**(17): 9282–9289. DOI: http://dx.doi.org/10.1021/es301138y.

White, AB, Mahoney, KM, Cifelli, R, King, C. 2015. Wind profilers to aid with monitoring and forecasting of high-impact weather in the southeastern and western United States. *Bull Amer Meteor Soc*. DOI: http://dx.doi.org/10.1175/BAMS-D-14-00170.1.

Worden, J, Wecht, K, Frankenberg, C, Alvarado, M, Bowman, K, Kort, E, Kulawik, S, Lee, M, Payne, V, Worden, H. 2013. CH_4 and CO distributions over tropical fires during October 2006 as observed by the Aura TES satellite instrument and modeled by GEOS-Chem. *Atmos Chem Phys* **13**: 3679–3692. DOI: http://dx.doi.org/10.5194/acp-13-3679-2013.

Wunch, D, Toon, GC, Wennberg, PO, Wofsy, SC, Stephens, BB, Fischer, ML, Uchino, O, Abshire, JB, Bernath, P, Biraud, SC, Blavier, J-FL, Boone, C, Bowman, KP, Browell, EV, Campos, T, Connor, BJ, Daube, BC, Deutscher, NM, Diao, M, Elkins, JW, Gerbig, C, Gottlieb, E, Griffith, DWT, Hurst, DF, Jiménez, R, Keppel-Aleks, G, Kort, EA, Macatangay, R, Machida, T, Matsueda, H, Moore, F, Morino, I, Park, S, Robinson, J, Roehl, CM, Sawa, Y, Sherlock, V, Sweeney, C, Tanaka, T, Zondlo, MA. 2010. Calibration of the Total Carbon Column Observing Network using aircraft profile data. *Atmos Meas Tech* **3**: 1351–1362. DOI: http://dx.doi.org/10.5194/amt-3-1351-2010.

Wunch, D, Wennberg, PO, Toon, GC, Connor, BJ, Fisher, B, Osterman, GB, Frankenberg, C, Mandrake, L, O'Dell, C, Ahonen, P, Biraud, SC, Castano, R, Cressie, N, Crisp, D, Deutscher, NM, Eldering, A, Fisher, ML, Griffith, DWT, Gunson, M, Heikkinen, P, Keppel-Aleks, G, Kyrö, E, Lindenmaier, R, Macatangay, R, Mendonca, J, Messerschmidt, J, Miller, CE, Morino, I, Notholt, J, Oyafuso, FA, Rettinger, M, Robinson, J, Roehl, CM, Salawitch, RJ, Sherlock, V, Strong, K, Sussmann, R, Tanaka, T, Thompson, DR, Uchino, O, Warneke, T, Wofsy, SC. 2011. A method for evaluating bias in global measurements of CO_2 total columns from space. *Atmos Chem Phys* **11**: 12317–12337. DOI: http://dx.doi.org/10.5194/acp-11-12317-2011.

Yacovitch, TI, Herndon, SC, Pétron, G, Kofler, J, Lyon, D, Zahniser, MS, Kolb, CE. 2015. Mobile laboratory observations of methane emissions in the Barnett Shale region. *Environ Sci Technol* **49**(13): 7889–7895. DOI: http://dx.doi.org/10.1021/es506352j.

Yacovitch, TI, Herndon, SC, Roscioli, JR, Floerchinger, C, McGovern, RM, Agnese, M, Pétron, G, Kofler, J, Sweeney, C, Karion, A, Conley, SA, Kort, EA, Nähle, L, Fischer, M, Hildebrandt, L, Koeth, J, McManus, JB, Nelson, DD, Zahniser, MS, Kolb, CE. 2014 Demonstration of an ethane spectrometer for methane source identification. *Environ Sci Technol* **48**(14): 8028–8034. DOI: http://dx.doi.org/10.1021/es501475q.

Zaimes, GG, Littlefield, JA, Augustine, DJ, Cooney, G, Schwietzke, S, George, FC, Lauderdale, T, Skone, TJ. 2019. Characterizing regional methane

emissions from natural gas liquid unloading. *Environ Sci Technol* **53**(8): 4619–4629. DOI: http://dx.doi.org/10.1021/acs.est.8b05546.

Zhang, M, Leifer, I, Hu, C. 2017. Challenges in methane column retrievals from AVIRIS-NG imagery over spectrally cluttered surfaces: A sensitivity analysis. *Remote Sensing* **9**(8): 835. DOI: http://dx.doi.org/10.3390/rs9080835.

Zickfeld, K, Solomon, S, Gilford, DM. 2017. Thermal sea-level rise due to short-lived gases. *Proc Natl Acad Sci USA* **114**(4): 657–662. DOI: http://dx.doi.org/10.1073/pnas.1612066114.

How to cite this article: Pétron, G, Miller, B, Vaughn, B, Thorley, E, Kofler, J, Mielke-Maday, I, Sherwood, O, Dlugokencky, E, Hall, B, Schwietzke, S, Conley, S, Peischl, J, Lang, P, Moglia, E, Crotwell, M, Crotwell, A, Sweeney, C, Newberger, T, Wolter, S, Kitzis, D, Bianco, L, King, C, Coleman, T, White, A, Rhodes, M, Tans, P, Schnell, R. 2020. Investigating large methane enhancements in the United States San Juan Basin. *Elem Sci Anth,* 8: xx. DOI: https://doi.org/10.1525/elementa.038

Domain Editor-in-Chief: Detlev Helmig, University of Colorado Boulder, CO, USA

Associate Editor: Brian Lamb, Washington State University, WA, USA

Knowledge Domain: Atmospheric Science

Part of an Elementa Forum: Oil and Natural Gas Development: Air Quality, Climate Science, and Policy

Published: 00, 0000 **Submitted:** March 30, 2020 **Accepted:** October 10, 2020

ELEMENTA Science of the Anthropocene

Elem Sci Anth is a peer-reviewed open access journal published by University of California Press.

OPEN ACCESS